This is a repository copy of *New Distortional Buckling Design Rules for Slotted Perforated Cold-Formed Steel Beams*.

White Rose Research Online URL for this paper:
http://eprints.whiterose.ac.uk/156229/

Version: Accepted Version

New Distortional Buckling Design Rules for Slotted Perforated Cold-Formed Steel Beams

Natalia Degtyareva

Institute of Architecture and Construction, South Ural State University,
Chelyabinsk, Russia

Perampalam Gatheeshgar

Faculty of Engineering and Environment, University of Northumbria,
Newcastle, UK.

Keerthan Poologanathan

Faculty of Engineering and Environment, University of Northumbria,
Newcastle, UK.

Shanmuganathan Gunalan

School of Engineering and Built Environment, Griffith University,
Gold Coast, QLD, 4222, Australia.

Konstantinos Daniel Tsavdaridis

School of Civil Engineering, Faculty of Engineering, University of Leeds
Leeds, UK.

Stephen Napper

Faculty of Engineering and Environment, University of Northumbria,
Newcastle, UK.

Abstract

Cold-Formed Steel (CFS) members with slotted perforations in webs are used in civil construction to amplify the thermal and energy performance of structures. However, the slotted webs reduce the structural performance of the element, prominently their shear, bending and combined bending and shear strengths. Many research studies have been undertaken to examine the behaviour of CFS channel sections subject to bending. Yet, no research has been performed to investigate the distortional buckling behaviour of slotted perforated CFS flexural members. Finite Element (FE) models of CFS channels with staggered slotted perforations were developed herein to investigate their distortional buckling under bending stress. A parametric study was conducted in detail by developing 432 slotted perforated CFS FE models based on the validation process with available experimental results. In particular, this paper presents the FE analysis details of CFS flexural members with slotted perforations subject to distortional buckling and results. The reliability of the current Direct Strength Method (DSM) for CFS flexural members with web holes subject to distortional buckling in accordance with the North American Specification (AISI S100) (2016) and the Australian/New Zealand

37 Standards (AS/NZ 4600) (2018) was investigated. Modified DSM formulae for slotted
38 perforated CFS flexural members subject to distortional buckling were also proposed.

39 *Keywords*: Cold-formed steel; Beam with Staggered Slotted Perforations; Ultimate Bending
40 Capacity; Finite Element Analyses; Direct Strength Method; Distortional Buckling

1 Introduction

42 Cold-Formed Steel (CFS) members have been extensively employed as load-bearing structural
43 members in low to mid-rise residential and commercial buildings and modular building
44 constructions. The advancements achieved in CFS manufacturing technologies have led to
45 modifications in CFS profiles. One such modification is CFS channels with staggered slotted
46 perforations (see Fig. 1). These slotted perforated channels have been preferred in light gauge
47 steel constructions to amplify the overall thermal, energy and fire performances [1-4]. The
48 aforementioned performance enhancements are achieved from the presence of staggered
49 slotted perforations in the web of CFS profiles which interrupt the direct heat flow path as
50 depicted in Fig. 2. Therefore, staggered slotted perforated CFS channels have proven their
51 promising advantages over solid web CFS channels and applicability in construction [1-4] (see
52 Fig. 3). However, the structural performance of these types of channels needs to be examined
53 thoroughly as the web perforations are more sensitive to the ultimate load-bearing capacities
54 of the CFS channels.

55 Previous studies have focused on investigating the compression, shear, and combined bending
56 and shear behaviour of slotted perforated CFS wall studs and beams. Kesti [5] performed
57 research on local and distortional buckling behaviour of slotted perforated wall studs and
58 proposed suitable design guidelines. The shear behaviour of slotted perforated CFS channels
59 has been investigated through structural tests [6] and numerical modelling [7] and it was found
60 that the ultimate shear capacity was reduced up to 70% due to the presence of slotted
61 perforations in the web. Degtyreva et al. [8] investigated the combined bending and shear
62 behaviour of slotted perforated CFS channels through the numerical analysis and presented
63 design proposals to predict the combined bending and shear capacity. Numerous experimental
64 and numerical research studies have been performed to study the flexural behaviour of C-
65 sections, Z-sections, and hollow flange sections with solid webs [9-16]. In addition, flexural
66 behaviour of CFS beams with conventional shape web holes have also been studied [17, 18]
67 and the Direct Strength Method (DSM) based design equations have been modified to consider
68 the effect of web holes on ultimate bending capacity. However, no research has been conducted
69 on the distortional and local buckling behaviours of CFS flexural members with staggered

70　　slotted web perforations to date, except some review about experimental studies in [19, 20].

71　　Hence, detailed research is carried out herein to assess the distortional buckling behaviour of

72　　CFS flexural members with staggered slotted perforated webs.

73　　Detailed information on the numerical studies of staggered slotted perforated CFS flexural

74　　members subject to distortional buckling is presented. Initially, CFS solid, rectangular web

75　　hole, and slotted web elements were modelled and the results were compared with the available

76　　experimental data to verify the model. Subsequently, a wide range of parametric studies was

77　　conducted and the results were used to extend the DSM based distortional buckling design

78　　equations for stagged slotted perforated CFS flexural members.

79　　**2　　Finite element modelling description and verification**

80　　The numerical models, with material and geometric nonlinearities, were constructed and

81　　analysed using a general-purpose Finite Element (FE) software, ANSYS [21]. FE specimen

82　　models were developed as simply supported four-point loading arrangement to ensure pure

83　　bending failure. Because of the symmetric nature of the loading arrangement, only half of the

84　　beam was modelled. FE models were analysed in two stages, linear elastic buckling analysis,

85　　and non-linear analysis, successively. The reported study utilized the supercomputer resources

86　　of South Ural State University. The supercomputer resources are the distributed memory

87　　parallel computers which resulted in a time efficiency of the performed FE analysis. The

88　　following sub-sections elaborate the detailed description on the FE model development.

89　　2.1　　Material modelling

90　　The non-linearity of the material in CFS beams was modelled with von Mises yield criteria

91　　along with isotropic hardening. The model consists of two components which are CFS channels

92　　and Web Side Plates (WSPs). The thin-walled CFS channel and 5 mm thickness of WSPs were

93　　modelled as bi-linear isotropic hardening (elastic-perfectly plastic) and elastic material,

94　　respectively. The modulus of the elasticity of the material is considered as 200 GPa, the

95　　Poisson's ratio was taken as 0.3 for both CFS channels and WSP. In general practice, both

96　　residual stresses and corner strength enhancements countereffect each other. Hence, both

97　　effects were not considered in the FE model development [22].

3

98   2.2   Element types

99   SHELL 181 element available in ANSYS [21] was used to model the CFS channels and WSPs.

100   This SHELL181 element has four nodes and each node is controlled with three translational

101   and three rotational degrees of freedom. This element is well-suited to simulate linear, large

102   rotation and large strain non-linear problems, thus can result in accurate predictions accounting

103   geometrical and material non-linearity of thin-walled CFS channels. The contact between WSP

104   and CFS channel was modelled with CONTA173 and TARGE170 elements.

105   2.3   Mesh control

106   The CFS channels and WSPs were meshed with quadrilateral element shapes. For greater

107   accuracy and efficiency of computing time, the solid segments (non-perforated regions) were

108   refined with a maximum mesh size of 5 mm × 5 mm. However, the slotted perforated regions

109   were provided with 1.5 mm × 5 mm mesh refinement, where 1.5 mm of maximum element

110   size in the vertical direction and 5 mm maximum element size in the longitudinal direction in

111   the perforated region. Similar mesh refinements were also used to study the shear [7] and

112   combined bending and shear [8] behaviour of slotted perforated CFS channels. Fig. 4 shows

113   the details of mesh refinements used in solid and slotted channels.

114   2.4   Geometric imperfections

115   The ultimate strength prediction and post-buckling behaviour of CFS thin-walled members

116   hugely rely on initial geometric imperfections [23]. Therefore, the inclusion of geometric

117   imperfections into the FE model is necessary. To account this, the imperfection shape and

118   magnitude were incorporated to the FE models via super positioning buckling modes which

119   were obtained from eigenvalue buckling analysis. The distortional buckling modes obtained in

120   elastic buckling analysis were selected to add the imperfection. The general form of

121   imperfection magnitude is given as a function of plate thickness or plate slenderness. Since the

122   main focus of this paper is to investigate the distortional buckling behaviour of CFS flexural

123   members with slotted perforations, imperfection magnitudes of 0.94t, 0.64t, and 0.15t (t = plate

124   thickness) were used as proposed in [23, 24]. Detailed description on the imperfections can be

125   found in the following sections.

4

126   2.5   Boundary conditions

127   Four-point loading simply supported boundary conditions were provided to the FE model. The

128   boundary conditions given to the CFS channels in the validation process are depicted in Figs.

129   5-7. Only half of the test set-up was simulated due to the symmetric nature of the four-point

130   loading bending test arrangement. The WSPs were the target surface and the CFS channels

131   were the contact surface. All the WSP nodes were restrained in the x-direction at the support

132   and loading point. The WSPs were connected to the CFS channels at the bolt locations through

133   coupling the WSP and CFS channel nodes in x-, y-, and z-directions. Strap locations were

134   simulated as boundary conditions by restraining the translation in the x-direction and the

135   rotation in the z-direction. The translation of the support WSP in y-direction was restrained at

136   the middle node of the bottom edge of the WSP. The nodes located at top edge of the loading

137   WSP were also coupled in the y-direction. The load was applied to the coupled node, where all

138   the vertical displacements are coupled, as displacement control approach.

139   2.6   Analysis procedure

140   The entire solution scheme has two phases: the elastic eigenvalue buckling analysis, and the

141   non-linear analysis. Initially, elastic eigenvalue buckling analysis was performed to the

142   developed FE models to generate the possible buckling modes. From that, the lowest

143   distortional buckling mode was used to input the shape and magnitude of the initial geometric

144   imperfection for non-linear analysis. The non-linear static analysis was used to obtain the

145   ultimate bending capacity subject to distortional buckling and the failure mode. This non-linear

146   analysis allows material yielding and large deformations when CFS beam subjected to loading

147   thus produces accurate results. The non-linear analysis was performed through sparse direct

148   equation solver.

149   2.7   FE Model verification

150   FE models were developed and verified against the available experiment results to ensure the

151   considered model characteristics are suitable for further study. Distortional buckling test results

152   of six solid web channels [25], three solid CFS channels and six CFS channels with rectangular

153   unstiffened web holes [17], and five CFS beams with slotted perforations [19] were used to

154   validate the FE models. Distortional buckling failure in the mid-span (pure bending zone) of

155   the four-point loading set-up was achieved by unrestraining the lateral translation of the

156   compression flange of CFS channels. Fig 4 shows the developed FE models for the validation

157   against test results while Figs. 5, 6 and 7 depict the provided boundary conditions to simulate

158   the actual test boundary conditions used in [25], [17] and [19] respectively. During this

159   verification process, three different imperfection magnitudes (0.94t, 0.64t, and 0.15t, where t

160   = plate thickness) with positive and negative values were used to determine the ultimate

161   capacity of the FE models. These positive and negative values represent the associated

162   distortional buckling modes of inward and outward movement of the top flange-lip juncture.

163   Table 1, Table 2 and Table 3 present the comparisons of the ultimate bending capacity results

164   subjected to distortional buckling failure obtained from the experiments (reported in [25], [17]

165   and [19] respectively) and FE analyses. Overall comparison of the test results and FE analysis

166   bending capacity predicted with different imperfection magnitude is provided in Table 4. From

167   Table 4, it can be noticed that the mean values of the test to FE ultimate capacity ratio for all

168   20 specimens show satisfactory agreement. Even though the imperfections were not measured

169   during the past distortional buckling tests [25, 17, 19] which are used for validation, the

170   selected imperfections magnitudes (0.15t, 0.64t and 0.94t) based on the proposals made by

171   Schafer and Pekoz [23] and Camotim and Silvestre [24] suited well to use in FE modelling.

172   Moreover, the selected imperfection magnitudes are within the manufacturing limits. Similar

173   imperfection magnitudes were also used in past research studies [13, 26]. To elaborate, it

174   provides a mean value of 1.03, 1.06, 1.02, 1.04, 0.98, and 0.98 for imperfection magnitudes of

175   0.94t, -0.94t, 0.64t,-0.64t, 0.15t, and -0.15t, respectively. In addition to that the coefficient of

176   variation (COV) values are 0.07 for 0.94t , 0.06 for -0.94t, 0.64t, -0.64t, and 0.15t, and 0.08 for

177   -0.15t imperfection magnitudes.

178   Table 1: Comparison of FE results and experimental [25] bending capacities of solid CFS channels

Sections	Test (kNm)	FE results for different imperfection magnitudes											
		0.94t		-0.94t		0.64t		-0.64t		0.15t		-0.15t	
		FE (kNm)	Test / FE	FE (kNm)	Test / FE	FE (kNm)	Test / FE	FE (kNm)	Test / FE	FE (kNm)	Test / FE	FE (kNm)	Test / FE
C15015-Mw	9.47	9.97	0.95	8.91	1.06	9.90	0.96	9.04	1.05	9.61	0.99	9.44	1.00
C15019-Mw	12.94	12.51	1.03	11.78	1.10	12.95	1.00	12.05	1.07	13.51	0.96	12.81	1.01
C15024-Mw	17.76	16.21	1.10	15.19	1.17	16.36	1.09	15.50	1.15	16.70	1.06	16.11	1.10
C20015-Mw	12.20	11.95	1.02	10.66	1.14	11.82	1.03	10.91	1.12	11.75	1.04	11.53	1.06
C20019-Mw	18.85	17.35	1.09	16.70	1.13	18.60	1.01	17.32	1.09	19.04	0.99	18.39	1.03
C20024-Mw	27.88	26.46	1.05	24.54	1.14	27.33	1.02	24.92	1.12	26.22	1.06	25.66	1.09
Min			0.95		1.06		0.96		1.05		0.96		1.00
Max			1.10		1.17		1.09		1.15		1.06		1.10
Mean			1.04		1.12		1.02		1.10		1.02		1.05
COV			0.05		0.03		0.04		0.03		0.04		0.04

179   Note: t = thickness

180

181

182

Table 2: Comparison of FE results and experimental [17] bending capacities of solid and rectangular web holed CFS channels

Sections	Test (kNm)	FE results for different imperfection magnitudes											
		0.94t		-0.94t		0.64t		-0.64t		0.15t		-0.15t	
		FE (kNm)	Test / FE	FE (kNm)	Test / FE	FE (kNm)	Test / FE	FE (kNm)	Test / FE	FE (kNm)	Test / FE	FE (kNm)	Test / FE
NH-1.1	12.6	12.06	1.05	12.06	1.04	12.15	1.04	12.35	1.02	13.52	0.93	14.42	0.87
NH-2.1	12.51	11.71	1.07	11.71	1.07	11.82	1.06	12.00	1.04	13.31	0.94	13.86	0.90
NH-3.2	13.02	11.92	1.09	11.92	1.09	12.03	1.08	12.21	1.07	13.49	0.97	14.19	0.92
H0.9-1.1	9.65	9.17	1.05	9.33	1.03	9.27	1.04	9.52	1.01	10.03	0.96	10.49	0.92
H0.9-2.2	10.54	9.58	1.10	9.83	1.07	9.76	1.08	10.12	1.04	11.29	0.93	11.62	0.91
H0.9-3.1	10.84	9.77	1.11	10.00	1.08	9.94	1.09	10.32	1.05	11.49	0.94	11.88	0.91
H0.8-1.2	8.19	8.34	0.98	8.44	0.97	8.55	0.96	8.63	0.95	9.03	0.91	9.20	0.89
H0.8-2.2	8.55	8.34	1.03	8.44	1.01	8.55	1.00	8.63	0.99	9.01	0.95	9.18	0.93
H0.8-3.2	8.56	8.53	1.00	8.62	0.99	8.73	0.98	8.81	0.97	9.25	0.93	9.38	0.91
Min			0.98		0.97		0.96		0.95		0.91		0.87
Max			1.11		1.09		1.09		1.07		0.97		0.93
Mean			1.05		1.04		1.04		1.02		0.94		0.91
COV			0.04		0.04		0.05		0.04		0.02		0.02

Note: t = thickness

Table 3: Comparison of FE results and experimental [19] bending capacities of slotted perforated CFS channels

Sections	Test (kNm)	FE results for different imperfection magnitudes											
		0.94t		-0.94t		0.64t		-0.64t		0.15t		-0.15t	
		FE (kNm)	Test / FE	FE (kNm)	Test / FE	FE (kNm)	Test / FE	FE (kNm)	Test / FE	FE (kNm)	Test / FE	FE (kNm)	Test / FE
PA-145-1.0	2.65	2.99	0.89	2.83	0.94	3.03	0.88	2.85	0.93	2.91	0.91	2.91	0.91
PA-145-1.5	5.42	5.72	0.95	5.00	1.08	5.78	0.94	5.08	1.07	5.40	1.00	5.19	1.04
PA-195-1.0	3.92	3.58	1.10	3.93	1.00	3.73	1.05	3.95	0.99	3.68	1.06	4.00	0.98
PA-195-1.5	6.80	7.58	0.90	6.58	1.03	6.81	1.00	6.61	1.03	7.59	0.90	6.67	1.02
PA-195-1.3	4.22	3.87	1.09	4.29	0.98	3.79	1.11	3.81	1.11	3.83	1.10	3.82	1.11
Min			0.89		0.94		0.88		0.93		0.90		0.91
Max			1.10		1.08		1.11		1.11		1.10		1.11
Mean			0.98		1.01		1.00		1.03		1.00		1.01
COV			0.10		0.05		0.09		0.07		0.09		0.07

Note: t = thickness

Table 4: Overall comparison of FE results and experimental [25, 17, 19] bending capacities of CFS channels

Sections	Overall Test /FE ratios for different imperfection magnitudes					
	Test/ FE$_{(0.94t)}$	Test/ FE$_{(-0.94t)}$	Test/ FE$_{(0.64t)}$	Test/ FE$_{(-0.64t)}$	Test/ FE$_{(0.15t)}$	Test/ FE$_{(-0.15t)}$
Min	0.89	0.94	0.88	0.93	0.90	0.87
Max	1.11	1.17	1.11	1.15	1.10	1.11
Mean	1.03	1.06	1.02	1.04	0.98	0.98
COV	0.07	0.06	0.06	0.06	0.06	0.08

Note: t = thickness

During the tests, the vertical displacement of the midpoint of the beam span was measured with the application of load. Similarly, in FE models the displacement of the midpoint of the beam span was obtained to ensure the test and FE deformations can be compared. Fig. 8 depicts the failure mode comparison between the FE analysis and test [26] for 150 mm deep channel with

195   1.9 mm thickness and without straps (C15019-Mw) while Fig. 9 shows the load-vertical

196   displacement behaviour obtained for the specimen C15019-Mw from the experiment [25] and

197   FE analysis. Both test and FE modelling load-vertical displacement have shown almost linear

198   response in Fig. 9 as this CFS section is relatively slender. In addition, this can cause sudden

199   elastic distortional buckling failure in mid-span. The aforementioned behaviour was observed

200   in tests by Pham and Hancock [25] and FE analysis in this study (see Fig. 8). This confirms

201   that the non-linear response is more likely to happen in stocky sections. The load-vertical

202   displacement behaviour for C15019-Mw shows consistent results at each stage in FE analysis

203   and test. The failure modes also depicted a high similarity between FE analysis and test.

204   Moreover, failure modes comparison between the test [17] and FE analysis for the specimens

205   with rectangular web openings is illustrated in Fig. 10. This comparison also showed similar

206   failure modes obtained in both cases of test and FE analysis. Overall, FE results for the CFS

207   flexural members which fail under distortional buckling agree well with that of the test results

208   in terms of (a) ultimate bending capacity; (b) load-vertical displacement behaviour and (c)

209   failure modes. This confirms that similar FE models characteristics including element types,

210   material model, and analysis type can be used to perform the parametric studies of CFS flexural

211   members with staggered slotted perforations subject to distortional buckling.

212   **3   Parametric studies**

213   This section presents the FE model details of the parametric study which was conducted to

214   investigate the distortional buckling failure behaviour of CFS flexural members. The

215   parametric study was aimed to create a wide range of data set and to develop improved design

216   guidelines to predict the ultimate bending capacity of CFS beams with staggered slotted

217   perforations subject to distortional buckling.

218   3.1   Varying parameters

219   After the validation process, a parametric study was conducted to create a wide range of results

220   base which can cover wider bounds. Therefore, the improved formula could be able to predict

221   the distortional buckling ultimate bending capacity of the staggered slotted perforated CFS

222   beams with different dimensional and mechanical properties. Therefore, section depth (D),

223   Flange width (B_f) (constant for particular section depth (D)), thickness (t), slot length (L_{sl}), slot

224   width (W_{sl}), number of slot rows (n), number of slot row groups (N) and yield strength (f_y)

225   were varied. Three different section depths of 150, 200, and 250 mm, two different flange

226   lengths of 45 and 65 mm, three different thicknesses of 1, 2, and 3 mm, two different slot length

227 of 60 and 75 mm, two different slot widths of 3 and 5 mm, three different slot rows of 6, 8, and

228 12 (6 rows for 150 mm section depth, 6 and 8 rows for 200 mm section depth, and 6, 8, and 12

229 rows for 250 mm section depth) , two-slot row groups and three different yield strength of 300,

230 500, and 600 MPa were considered in the parametric study. The varying parameters are

231 presented in Table 5. A total number of 432 FE models were developed and analysed for this

232 parametric study considering the aforementioned influencing parameters. The labelling rule for

233 the FE models developed for the parametric study is illustrated in Fig.11.

234

235
<center>Table 5: Parametric study details</center>

f_y (MPa)	D (mm)	B_f (mm)	B_l (mm)	t (mm)	L_{sl} (mm)	W_{sl} (mm)	n	N	Number of models
300	150	45	13	1, 2, 3	60, 75	3, 5	6	1, 2	24
	200	45	13	1, 2, 3	60, 75	3, 5	6, 8	1, 2	48
	250	65	13	1, 2, 3	60, 75	3, 5	6, 8, 12	1, 2	72
Sub-total									144
500	150	45	13	1, 2, 3	60, 75	3, 5	6	1, 2	24
	200	45	13	1, 2, 3	60, 75	3, 5	6, 8	1, 2	48
	250	65	13	1, 2, 3	60, 75	3, 5	6, 8, 12	1, 2	72
Sub-total									144
600	150	45	13	1, 2, 3	60, 75	3, 5	6	1, 2	24
	200	45	13	1, 2, 3	60, 75	3, 5	6, 8	1, 2	48
	250	65	13	1, 2, 3	60, 75	3, 5	6, 8, 12	1, 2	72
Sub-total									144
Total									432

236 Note: f_y = yield stress, D = section depth, B_f = flange width, B_l = lip length, t = thickness, L_{sl} = slot length, W_{sl} = slot width,

237 n = number of slot rows, N = number of slot row groups

238 ## 3.2   Selection of FE model span

239 The validated FE models have the total span of 2600, 4800, and 3950 mm as similar to test

240 spans which were reported in [25], [17], and [19], respectively. For the parametric study, it is

241 essential to select one span. Therefore, a few analyses were performed to evaluate the influence

242 of the total span on the ultimate bending capacity of the CFS beams with staggered slotted

243 perforations. For same dimensions of the CFS beams, the analysis was conducted in two

244 options: (a) CFS beams having the span of 4800 mm and staggered slotted perforations

245 incorporated in the entire web of the span (see Fig. 12); (b) CFS beams having the span of 2600

246 mm and staggered slotted perforations incorporated only in web of the mid-span (see Fig. 13).

247 The boundary conditions used for these two options are depicted in Figs. 14 and 15,

248 respectively. The ultimate bending capacity obtained from the FE analysis for these two cases

249 were compared and the results are presented in Table 6. Figs. 16-18 shows the failure modes
250 comparison obtained at different stages for these short and long span channels. The results
251 showed that the span and providing slotted perforation in two end spans of the four-point
252 loading arrangement do not influence the ultimate bending capacity. Therefore, the span of
253 2600 mm with staggered slotted perforations provided only in the mid-span (option (b)) was
254 used for the parametric study because the shorter span consumes less computational time
255 compared to the larger span and the solid shear span in the shorter beam prevents the combined
256 bending and shear failure.

257 Moreover, Pham and Hancock [25] and Moen et al. [17] used different mid-span lengths of
258 1000 mm and 1626 mm, respectively in their four-point test set-ups. The performed analysis
259 to investigate the influence of the total span of the four-point set-up also confirm the different
260 lengths for mid-span (option (a): mid-span is 1626 mm, and option (b): mid-span is 1000 mm
261) have no influence on the ultimate bending capacity prediction. Hence, the consideration of
262 the ratio between mid-span and the distortional buckling half wavelength is likely to be
263 neglected.

264   Table 6: FE ultimate bending capacity comparison for slotted CFS channels having different spans.

FE model	$M_{slots, 4.8}$ (kNm)	$M_{slots, 2.6}$ (kNm)	$M_{slots, 4.8} / M_{slots, 2.6}$
150-1-60-3-1-6-600	3.88	3.85	1.01
150-1-60-3-2-6-600	3.47	3.44	1.01
150-3-60-3-1-6-600	16.02	15.94	1.01
150-3-60-3-2-6-600	15.45	15.35	1.01
250-1-60-3-1-6-600	6.22	6.20	1.00
250-1-60-3-2-6-600	6.16	6.15	1.00
250-1-60-3-1-12-600	6.04	6.06	1.00
250-1-60-3-2-12-600	5.79	5.76	1.00
250-3-60-3-1-6-600	36.11	36.02	1.00
250-3-60-3-2-6-600	35.59	35.56	1.00
250-3-60-3-1-12-600	34.77	34.74	1.00
250-3-60-3-2-12-600	33.41	33.36	1.00
150-1-60-3-1-6-300	2.74	2.73	1.00
150-1-60-3-2-6-300	2.57	2.58	1.00
150-3-60-3-1-6-300	9.23	9.20	1.00
150-3-60-3-2-6-300	9.05	9.00	1.01
250-1-60-3-1-6-300	4.81	4.80	1.00
250-1-60-3-2-6-300	4.73	4.79	0.99
250-1-60-3-1-12-300	4.63	4.65	1.00
250-1-60-3-2-12-300	4.42	4.40	1.01
250-3-60-3-1-6-300	22.15	22.10	1.00
250-3-60-3-2-6-300	21.82	21.81	1.00
250-3-60-3-1-12-300	21.35	21.33	1.00
250-3-60-3-2-12-300	20.71	20.72	1.00

265   Note: $M_{slots, 4.8}$ = bending capacity for 4800 mm span, $M_{slots, 2.6}$ = bending capacity for 2600 mm span

4   Results analysis of the parametric study

The flexural behaviour of CFS beams with staggered slotted perforations was investigated in detail using 432 FE parametric models. In addition to that the bending capacity of the corresponding solid web channels (without slotted perforations) were also obtained from FE as a reference and those results were required to propose improved design guidelines as explained in following sections. Figs 19a and 19b show the von Mises stress failure modes of the 150 mm section depth CFS solid web channels and the corresponding failure modes when staggered slotted perforations are provided. In addition to that deformation failure patterns obtained from the FE analysis for the staggered slotted perforated CFS channels are depicted in Fig. 20. Table 7 summarises the distortional buckling moments, section and elastic properties of the solid web channels. The entire parametric study results of bending capacity for the staggered slotted perforations and the corresponding capacities for the solid CFS channels are presented in Table 8-10 for 300, 500, and 600 MPa yield strengths, respectively. Here M_{solid} is the flexural capacity of the solid CFS channels and the M_{slots} is the flexural capacity of the staggered slotted channels subjected to distortional buckling. The reduction factor, which is the ratio between the bending capacity of the staggered slotted channel and the corresponding bending capacity of the solid CFS channel are also presented in Table 8-10 for all 432 Fe models. Overall, it can be noticed up to 23% of bending capacity reduction was noticed and this occurs when web experiences the highest web area reduction. The small capacity reduction was noticed when the CFS channel web experiences the lowest area reduction due to the slotted perforations. Moreover, CFS channels with two-row groups of slotted perforations resulted in a higher bending capacity reduction than similar CFS channels with single row groups of slotted perforations when other parameters remain the same. This behaviour can be argued that the slotted perforations are subjected to higher compressive stress as the slots are placed near the compression flange in the case of two slot row groups, but near the neutral axis in the case of single-slot row group. The variation of the reduction factor against the considered influencing parameters is plotted in Fig. 21.

293 Table 7: Section and elastic properties of the solid web CFS channels

D (mm)	B_f (mm)	B_l (mm)	t (mm)	Z (mm³)	S (mm³)	S/Z	M_{od} (kNm)	λ_d fy=300 MPa	fy=500 MPa	fy=600 MPa
150	45	13	1	11 416	13 812	1.21	3.52	0.99	1.27	1.39
			2	21 416	26 945	1.26	15.12	0.65	0.84	0.92
			3	30 024	39 404	1.31	37.16	0.49	0.64	0.70
200	45	13	1	17 018	20 987	1.23	3.81	1.16	1.49	1.64
			2	32 199	41 094	1.28	16.90	0.76	0.98	1.07
			3	45 567	60 329	1.32	43.39	0.57	0.73	0.80
250	65	13	1	28 416	34 393	1.21	3.65	1.51	1.95	2.14
			2	54 495	67 644	1.24	16.38	0.99	1.28	1.40
			3	78 260	99 824	1.28	41.74	0.75	0.97	1.06
Mean						1.26				

294 Note: D = section depth, B_f = flange width, B_l = lip length, Z = elastic section modulus, S = plastic section modulus, M_{od} =
295 distortional buckling moment, λ_d = distortional buckling slenderness based on yield and distortional buckling
296 moment

297

298 Table 8: Parametric study results for f_y = 300 MPa

No	Channels with Slotted Webs	M_{slots} (kNm)	M_{solid} (kNm)	M_{slots}/M_{solid}	No	Channels with Slotted Webs	M_{slots} (kNm)	M_{solid} (kNm)	M_{slots}/M_{solid}
1	150-1-60-3-1-6-300	2.73	2.95	0.93	73	250-1-60-3-1-6-300	4.82	4.93	0.98
2	150-1-60-5-1-6-300	2.66	2.95	0.90	74	250-1-60-5-1-6-300	4.83	4.93	0.98
3	150-1-75-3-1-6-300	2.64	2.95	0.90	75	250-1-75-3-1-6-300	4.80	4.93	0.97
4	150-1-75-5-1-6-300	2.55	2.95	0.87	76	250-1-75-5-1-6-300	4.72	4.93	0.96
5	150-1-60-3-2-6-300	2.58	2.95	0.88	77	250-1-60-3-2-6-300	4.79	4.93	0.97
6	150-1-60-5-2-6-300	2.40	2.95	0.82	78	250-1-60-5-2-6-300	4.74	4.93	0.96
7	150-1-75-3-2-6-300	2.44	2.95	0.83	79	250-1-75-3-2-6-300	4.72	4.93	0.96
8	150-1-75-5-2-6-300	2.30	2.95	0.78	80	250-1-75-5-2-6-300	4.68	4.93	0.95
9	150-2-60-3-1-6-300	6.09	6.44	0.95	81	250-1-60-3-1-8-300	4.80	4.93	0.97
10	150-2-60-5-1-6-300	5.99	6.44	0.93	82	250-1-60-5-1-8-300	4.76	4.93	0.97
11	150-2-75-3-1-6-300	5.96	6.44	0.93	83	250-1-75-3-1-8-300	4.74	4.93	0.96
12	150-2-75-5-1-6-300	5.86	6.44	0.91	84	250-1-75-5-1-8-300	4.66	4.93	0.94
13	150-2-60-3-2-6-300	5.90	6.44	0.92	85	250-1-60-3-2-8-300	4.71	4.93	0.95
14	150-2-60-5-2-6-300	5.75	6.44	0.89	86	250-1-60-5-2-8-300	4.68	4.93	0.95
15	150-2-75-3-2-6-300	5.80	6.44	0.90	87	250-1-75-3-2-8-300	4.60	4.93	0.93
16	150-2-75-5-2-6-300	5.64	6.44	0.88	88	250-1-75-5-2-8-300	4.52	4.93	0.92
17	150-3-60-3-1-6-300	9.20	9.53	0.96	89	250-1-60-3-1-12-300	4.65	4.93	0.94
18	150-3-60-5-1-6-300	9.10	9.53	0.95	90	250-1-60-5-1-12-300	4.60	4.93	0.93
19	150-3-75-3-1-6-300	9.42	9.53	0.99	91	250-1-75-3-1-12-300	4.57	4.93	0.93
20	150-3-75-5-1-6-300	9.32	9.53	0.98	92	250-1-75-5-1-12-300	4.49	4.93	0.91
21	150-3-60-3-2-6-300	9.00	9.53	0.94	93	250-1-60-3-2-12-300	4.40	4.93	0.89
22	150-3-60-5-2-6-300	8.83	9.53	0.93	94	250-1-60-5-2-12-300	4.36	4.93	0.88
23	150-3-75-3-2-6-300	9.22	9.53	0.97	95	250-1-75-3-2-12-300	4.31	4.93	0.87
24	150-3-75-5-2-6-300	9.03	9.53	0.95	96	250-1-75-5-2-12-300	4.23	4.93	0.86
25	200-1-60-3-1-6-300	3.86*	3.86	1.00	97	250-2-60-3-1-6-300	13.61	13.70	0.99
26	200-1-60-5-1-6-300	3.81	3.86	0.99	98	250-2-60-5-1-6-300	13.54	13.70	0.99
27	200-1-75-3-1-6-300	3.74	3.86	0.97	99	250-2-75-3-1-6-300	13.48	13.70	0.98
28	200-1-75-5-1-6-300	3.69	3.86	0.96	100	250-2-75-5-1-6-300	13.34	13.70	0.97
29	200-1-60-3-2-6-300	3.68	3.86	0.95	101	250-2-60-3-2-6-300	13.42	13.70	0.98
30	200-1-60-5-2-6-300	3.63	3.86	0.94	102	250-2-60-5-2-6-300	13.38	13.70	0.98
31	200-1-75-3-2-6-300	3.60	3.86	0.93	103	250-2-75-3-2-6-300	13.31	13.70	0.97
32	200-1-75-5-2-6-300	3.54	3.86	0.92	104	250-2-75-5-2-6-300	13.21	13.70	0.96
33	200-1-60-3-1-8-300	3.72	3.86	0.96	105	250-2-60-3-1-8-300	13.48	13.70	0.98
34	200-1-60-5-1-8-300	3.67	3.86	0.95	106	250-2-60-5-1-8-300	13.41	13.70	0.98
35	200-1-75-3-1-8-300	3.75	3.86	0.97	107	250-2-75-3-1-8-300	13.32	13.70	0.97

No		M_slots	M_solid	M_slots / M_solid	No		M_slots	M_solid	M_slots / M_solid
36	200-1-75-5-1-8-300	3.71	3.86	0.96	108	250-2-75-5-1-8-300	13.19	13.70	0.96
37	200-1-60-3-2-8-300	3.56	3.86	0.92	109	250-2-60-3-2-8-300	13.22	13.70	0.97
38	200-1-60-5-2-8-300	3.48	3.86	0.90	110	250-2-60-5-2-8-300	13.16	13.70	0.96
39	200-1-75-3-2-8-300	3.45	3.86	0.89	111	250-2-75-3-2-8-300	13.12	13.70	0.96
40	200-1-75-5-2-8-300	3.33	3.86	0.86	112	250-2-75-5-2-8-300	13.00	13.70	0.95
41	200-2-60-3-1-6-300	8.87	9.03	0.98	113	250-2-60-3-1-12-300	13.11	13.70	0.96
42	200-2-60-5-1-6-300	8.77	9.03	0.97	114	250-2-60-5-1-12-300	13.01	13.70	0.95
43	200-2-75-3-1-6-300	8.69	9.03	0.96	115	250-2-75-3-1-12-300	12.95	13.70	0.95
44	200-2-75-5-1-6-300	8.56	9.03	0.95	116	250-2-75-5-1-12-300	12.75	13.70	0.93
45	200-2-60-3-2-6-300	8.61	9.03	0.95	117	250-2-60-3-2-12-300	12.68	13.70	0.93
46	200-2-60-5-2-6-300	8.51	9.03	0.94	118	250-2-60-5-2-12-300	12.36	13.70	0.90
47	200-2-75-3-2-6-300	8.44	9.03	0.93	119	250-2-75-3-2-12-300	12.44	13.70	0.91
48	200-2-75-5-2-6-300	8.31	9.03	0.92	120	250-2-75-5-2-12-300	11.96	13.70	0.87
49	200-2-60-3-1-8-300	8.70	9.03	0.96	121	250-3-60-3-1-6-300	22.13	22.66	0.98
50	200-2-60-5-1-8-300	8.59	9.03	0.95	122	250-3-60-5-1-6-300	22.02	22.66	0.97
51	200-2-75-3-1-8-300	8.50	9.03	0.94	123	250-3-75-3-1-6-300	22.56	22.66	0.99
52	200-2-75-5-1-8-300	8.36	9.03	0.93	124	250-3-75-5-1-6-300	22.38	22.66	0.99
53	200-2-60-3-2-8-300	8.37	9.03	0.93	125	250-3-60-3-2-6-300	21.84	22.66	0.96
54	200-2-60-5-2-8-300	8.26	9.03	0.91	126	250-3-60-5-2-6-300	21.69	22.66	0.96
55	200-2-75-3-2-8-300	8.20	9.03	0.91	127	250-3-75-3-2-6-300	22.22	22.66	0.98
56	200-2-75-5-2-8-300	8.09	9.03	0.90	128	250-3-75-5-2-6-300	22.02	22.66	0.97
57	200-3-60-3-1-6-300	13.80	13.86	1.00	129	250-3-60-3-1-8-300	22.01	22.66	0.97
58	200-3-60-5-1-6-300	13.73	13.86	0.99	130	250-3-60-5-1-8-300	21.81	22.66	0.96
59	200-3-75-3-1-6-300	13.96	13.86	1.01*	131	250-3-75-3-1-8-300	22.32	22.66	0.98
60	200-3-75-5-1-6-300	13.87	13.86	1.00*	132	250-3-75-5-1-8-300	22.07	22.66	0.97
61	200-3-60-3-2-6-300	13.60	13.86	0.98	133	250-3-60-3-2-8-300	21.52	22.66	0.95
62	200-3-60-5-2-6-300	13.50	13.86	0.97	134	250-3-60-5-2-8-300	21.34	22.66	0.94
63	200-3-75-3-2-6-300	13.74	13.86	0.99	135	250-3-75-3-2-8-300	21.87	22.66	0.97
64	200-3-75-5-2-6-300	13.56	13.86	0.98	136	250-3-75-5-2-8-300	21.62	22.66	0.95
65	200-3-60-3-1-8-300	13.66	13.86	0.99	137	250-3-60-3-1-12-300	21.38	22.66	0.94
66	200-3-60-5-1-8-300	13.58	13.86	0.98	138	250-3-60-5-1-12-300	21.12	22.66	0.93
67	200-3-75-3-1-8-300	13.75	13.86	0.99	139	250-3-75-3-1-12-300	21.61	22.66	0.95
68	200-3-75-5-1-8-300	13.63	13.86	0.98	140	250-3-75-5-1-12-300	21.28	22.66	0.94
69	200-3-60-3-2-8-300	13.37	13.86	0.96	141	250-3-60-3-2-12-300	20.74	22.66	0.92
70	200-3-60-5-2-8-300	13.21	13.86	0.95	142	250-3-60-5-2-12-300	20.40	22.66	0.90
71	200-3-75-3-2-8-300	13.39	13.86	0.97	143	250-3-75-3-2-12-300	20.96	22.66	0.92
72	200-3-75-5-2-8-300	13.20	13.86	0.95	144	250-3-75-5-2-12-300	20.42	22.66	0.90

299   Note: M_{slots} = bending capacity of slotted web channel, M_{solid} = bending capacity of solid web channel, * = numerical errors

300

301   Table 9: Parametric study results for f_y = 500 MPa

No	Channels with Slotted Webs	M_{slots} (kNm)	M_{solid} (kNm)	M_{slots} / M_{solid}	No	Channels with Slotted Webs	M_{slots} (kNm)	M_{solid} (kNm)	M_{slots} / M_{solid}
1	150-1-60-3-1-6-500	3.65	3.85	0.95	73	250-1-60-3-1-6-500	5.73	5.94	0.96
2	150-1-60-5-1-6-500	3.54	3.85	0.92	74	250-1-60-5-1-6-500	5.76	5.94	0.97
3	150-1-75-3-1-6-500	3.52	3.85	0.91	75	250-1-75-3-1-6-500	5.75	5.94	0.97
4	150-1-75-5-1-6-500	3.36	3.85	0.87	76	250-1-75-5-1-6-500	5.71	5.94	0.96
5	150-1-60-3-2-6-500	3.23	3.85	0.84	77	250-1-60-3-2-6-500	5.75	5.94	0.97
6	150-1-60-5-2-6-500	3.08	3.85	0.80	78	250-1-60-5-2-6-500	5.71	5.94	0.96
7	150-1-75-3-2-6-500	3.16	3.85	0.82	79	250-1-75-3-2-6-500	5.68	5.94	0.96
8	150-1-75-5-2-6-500	2.97	3.85	0.77	80	250-1-75-5-2-6-500	5.64	5.94	0.95
9	150-2-60-3-1-6-500	8.88	9.53	0.93	81	250-1-60-3-1-8-500	5.79	5.94	0.98
10	150-2-60-5-1-6-500	8.71	9.53	0.91	82	250-1-60-5-1-8-500	5.76	5.94	0.97
11	150-2-75-3-1-6-500	8.60	9.53	0.90	83	250-1-75-3-1-8-500	5.73	5.94	0.97
12	150-2-75-5-1-6-500	8.43	9.53	0.88	84	250-1-75-5-1-8-500	5.69	5.94	0.96
13	150-2-60-3-2-6-500	8.46	9.53	0.89	85	250-1-60-3-2-8-500	5.69	5.94	0.96
14	150-2-60-5-2-6-500	8.20	9.53	0.86	86	250-1-60-5-2-8-500	5.64	5.94	0.95
15	150-2-75-3-2-6-500	8.23	9.53	0.86	87	250-1-75-3-2-8-500	5.62	5.94	0.95

13

		M_{slots}	M_{solid}				M_{slots}	M_{solid}	
16	150-2-75-5-2-6-500	7.89	9.53	0.83	88	250-1-75-5-2-8-500	5.48	5.94	0.92
17	150-3-60-3-1-6-500	13.91	14.71	0.95	89	250-1-60-3-1-12-500	5.62	5.94	0.95
18	150-3-60-5-1-6-500	13.70	14.71	0.93	90	250-1-60-5-1-12-500	5.58	5.94	0.94
19	150-3-75-3-1-6-500	14.13	14.71	0.96	91	250-1-75-3-1-12-500	5.54	5.94	0.93
20	150-3-75-5-1-6-500	13.92	14.71	0.95	92	250-1-75-5-1-12-500	5.49	5.94	0.92
21	150-3-60-3-2-6-500	13.46	14.71	0.91	93	250-1-60-3-2-12-500	5.37	5.94	0.90
22	150-3-60-5-2-6-500	13.11	14.71	0.89	94	250-1-60-5-2-12-500	5.29	5.94	0.89
23	150-3-75-3-2-6-500	13.67	14.71	0.93	95	250-1-75-3-2-12-500	5.24	5.94	0.88
24	150-3-75-5-2-6-500	13.29	14.71	0.90	96	250-1-75-5-2-12-500	5.18	5.94	0.87
25	200-1-60-3-1-6-500	5.18	5.06	1.02[*]	97	250-2-60-3-1-6-500	18.92	19.09	0.99
26	200-1-60-5-1-6-500	5.12	5.06	1.01[*]	98	250-2-60-5-1-6-500	18.83	19.09	0.99
27	200-1-75-3-1-6-500	5.07	5.06	1.00[*]	99	250-2-75-3-1-6-500	18.68	19.09	0.98
28	200-1-75-5-1-6-500	5.01	5.06	0.99	100	250-2-75-5-1-6-500	18.61	19.09	0.97
29	200-1-60-3-2-6-500	4.97	5.06	0.98	101	250-2-60-3-2-6-500	18.79	19.09	0.98
30	200-1-60-5-2-6-500	4.90	5.06	0.97	102	250-2-60-5-2-6-500	18.69	19.09	0.98
31	200-1-75-3-2-6-500	4.88	5.06	0.96	103	250-2-75-3-2-6-500	18.61	19.09	0.97
32	200-1-75-5-2-6-500	4.75	5.06	0.94	104	250-2-75-5-2-6-500	18.49	19.09	0.97
33	200-1-60-3-1-8-500	5.01	5.06	0.99	105	250-2-60-3-1-8-500	18.89	19.09	0.99
34	200-1-60-5-1-8-500	4.95	5.06	0.98	106	250-2-60-5-1-8-500	18.72	19.09	0.98
35	200-1-75-3-1-8-500	5.08	5.06	1.00[*]	107	250-2-75-3-1-8-500	18.66	19.09	0.98
36	200-1-75-5-1-8-500	4.90	5.06	0.97	108	250-2-75-5-1-8-500	18.52	19.09	0.97
37	200-1-60-3-2-8-500	4.79	5.06	0.95	109	250-2-60-3-2-8-500	18.58	19.09	0.97
38	200-1-60-5-2-8-500	4.62	5.06	0.91	110	250-2-60-5-2-8-500	18.42	19.09	0.96
39	200-1-75-3-2-8-500	4.59	5.06	0.91	111	250-2-75-3-2-8-500	18.35	19.09	0.96
40	200-1-75-5-2-8-500	4.40	5.06	0.87	112	250-2-75-5-2-8-500	18.26	19.09	0.96
41	200-2-60-3-1-6-500	12.70	12.94	0.98	113	250-2-60-3-1-12-500	18.42	19.09	0.96
42	200-2-60-5-1-6-500	12.57	12.94	0.97	114	250-2-60-5-1-12-500	18.23	19.09	0.95
43	200-2-75-3-1-6-500	12.46	12.94	0.96	115	250-2-75-3-1-12-500	18.15	19.09	0.95
44	200-2-75-5-1-6-500	12.28	12.94	0.95	116	250-2-75-5-1-12-500	17.85	19.09	0.93
45	200-2-60-3-2-6-500	12.32	12.94	0.95	117	250-2-60-3-2-12-500	17.72	19.09	0.93
46	200-2-60-5-2-6-500	12.15	12.94	0.94	118	250-2-60-5-2-12-500	16.96	19.09	0.89
47	200-2-75-3-2-6-500	12.03	12.94	0.93	119	250-2-75-3-2-12-500	17.01	19.09	0.89
48	200-2-75-5-2-6-500	11.84	12.94	0.92	120	250-2-75-5-2-12-500	16.08	19.09	0.84
49	200-2-60-3-1-8-500	12.46	12.94	0.96	121	250-3-60-3-1-6-500	31.95	32.64	0.98
50	200-2-60-5-1-8-500	12.30	12.94	0.95	122	250-3-60-5-1-6-500	31.83	32.64	0.98
51	200-2-75-3-1-8-500	12.16	12.94	0.94	123	250-3-75-3-1-6-500	32.19	32.64	0.99
52	200-2-75-5-1-8-500	11.97	12.94	0.93	124	250-3-75-5-1-6-500	31.90	32.64	0.98
53	200-2-60-3-2-8-500	11.93	12.94	0.92	125	250-3-60-3-2-6-500	31.53	32.64	0.97
54	200-2-60-5-2-8-500	11.73	12.94	0.91	126	250-3-60-5-2-6-500	31.35	32.64	0.96
55	200-2-75-3-2-8-500	11.62	12.94	0.90	127	250-3-75-3-2-6-500	31.68	32.64	0.97
56	200-2-75-5-2-8-500	11.44	12.94	0.88	128	250-3-75-5-2-6-500	31.38	32.64	0.96
57	200-3-60-3-1-6-500	20.66	20.76	0.99	129	250-3-60-3-1-8-500	31.75	32.64	0.97
58	200-3-60-5-1-6-500	20.54	20.76	0.99	130	250-3-60-5-1-8-500	31.52	32.64	0.97
59	200-3-75-3-1-6-500	20.82	20.76	1.00[*]	131	250-3-75-3-1-8-500	31.81	32.64	0.97
60	200-3-75-5-1-6-500	20.62	20.76	0.99	132	250-3-75-5-1-8-500	31.45	32.64	0.96
61	200-3-60-3-2-6-500	20.18	20.76	0.97	133	250-3-60-3-2-8-500	31.06	32.64	0.95
62	200-3-60-5-2-6-500	19.93	20.76	0.96	134	250-3-60-5-2-8-500	30.80	32.64	0.94
63	200-3-75-3-2-6-500	20.28	20.76	0.98	135	250-3-75-3-2-8-500	31.12	32.64	0.95
64	200-3-75-5-2-6-500	19.96	20.76	0.96	136	250-3-75-5-2-8-500	30.76	32.64	0.94
65	200-3-60-3-1-8-500	20.33	20.76	0.98	137	250-3-60-3-1-12-500	30.78	32.64	0.94
66	200-3-60-5-1-8-500	20.13	20.76	0.97	138	250-3-60-5-1-12-500	30.44	32.64	0.93
67	200-3-75-3-1-8-500	20.36	20.76	0.98	139	250-3-75-3-1-12-500	30.71	32.64	0.94
68	200-3-75-5-1-8-500	20.11	20.76	0.97	140	250-3-75-5-1-12-500	30.29	32.64	0.93
69	200-3-60-3-2-8-500	19.53	20.76	0.94	141	250-3-60-3-2-12-500	29.62	32.64	0.91
70	200-3-60-5-2-8-500	19.22	20.76	0.93	142	250-3-60-5-2-12-500	29.01	32.64	0.89
71	200-3-75-3-2-8-500	19.61	20.76	0.94	143	250-3-75-3-2-12-500	29.52	32.64	0.90
72	200-3-75-5-2-8-500	19.28	20.76	0.93	144	250-3-75-5-2-12-500	28.32	32.64	0.87

302   Note: M_{slots} = bending capacity of slotted web channel, M_{solid} = bending capacity of solid web channel, * = numerical errors

303

Table 10: Parametric study results for $f_y = 600$ MPa

No	Channels with Slotted Webs	M_{slots} (kNm)	M_{solid} (kNm)	M_{slots}/M_{solid}	No	Channels with Slotted Webs	M_{slots} (kNm)	M_{solid} (kNm)	M_{slots}/M_{solid}
1	150-1-60-3-1-6-600	3.85	4.06	0.95	73	250-1-60-3-1-6-600	6.05	6.33	0.95
2	150-1-60-5-1-6-600	3.75	4.06	0.92	74	250-1-60-5-1-6-600	6.13	6.33	0.97
3	150-1-75-3-1-6-600	3.72	4.06	0.92	75	250-1-75-3-1-6-600	6.12	6.33	0.97
4	150-1-75-5-1-6-600	3.58	4.06	0.88	76	250-1-75-5-1-6-600	6.09	6.33	0.96
5	150-1-60-3-2-6-600	3.44	4.06	0.85	77	250-1-60-3-2-6-600	6.18	6.33	0.98
6	150-1-60-5-2-6-600	3.29	4.06	0.81	78	250-1-60-5-2-6-600	6.14	6.33	0.97
7	150-1-75-3-2-6-600	3.35	4.06	0.82	79	250-1-75-3-2-6-600	6.11	6.33	0.97
8	150-1-75-5-2-6-600	3.19	4.06	0.78	80	250-1-75-5-2-6-600	6.07	6.33	0.96
9	150-2-60-3-1-6-600	10.04	10.80	0.93	81	250-1-60-3-1-8-600	6.22	6.33	0.98
10	150-2-60-5-1-6-600	9.84	10.80	0.91	82	250-1-60-5-1-8-600	6.18	6.33	0.98
11	150-2-75-3-1-6-600	9.72	10.80	0.90	83	250-1-75-3-1-8-600	6.16	6.33	0.97
12	150-2-75-5-1-6-600	9.51	10.80	0.88	84	250-1-75-5-1-8-600	6.12	6.33	0.97
13	150-2-60-3-2-6-600	9.51	10.80	0.88	85	250-1-60-3-2-8-600	6.12	6.33	0.97
14	150-2-60-5-2-6-600	9.13	10.80	0.84	86	250-1-60-5-2-8-600	6.07	6.33	0.96
15	150-2-75-3-2-6-600	9.19	10.80	0.85	87	250-1-75-3-2-8-600	6.05	6.33	0.96
16	150-2-75-5-2-6-600	8.61	10.80	0.80	88	250-1-75-5-2-8-600	5.88	6.33	0.93
17	150-3-60-3-1-6-600	15.94	16.91	0.94	89	250-1-60-3-1-12-600	6.05	6.33	0.96
18	150-3-60-5-1-6-600	15.69	16.91	0.93	90	250-1-60-5-1-12-600	6.00	6.33	0.95
19	150-3-75-3-1-6-600	16.16	16.91	0.96	91	250-1-75-3-1-12-600	5.97	6.33	0.94
20	150-3-75-5-1-6-600	15.90	16.91	0.94	92	250-1-75-5-1-12-600	5.93	6.33	0.94
21	150-3-60-3-2-6-600	15.35	16.91	0.91	93	250-1-60-3-2-12-600	5.78	6.33	0.91
22	150-3-60-5-2-6-600	14.90	16.91	0.88	94	250-1-60-5-2-12-600	5.69	6.33	0.90
23	150-3-75-3-2-6-600	15.54	16.91	0.92	95	250-1-75-3-2-12-600	5.66	6.33	0.89
24	150-3-75-5-2-6-600	15.04	16.91	0.89	96	250-1-75-5-2-12-600	5.60	6.33	0.88
25	200-1-60-3-1-6-600	5.49	5.37	1.02*	97	250-2-60-3-1-6-600	20.98	21.22	0.99
26	200-1-60-5-1-6-600	5.45	5.37	1.01*	98	250-2-60-5-1-6-600	20.93	21.22	0.99
27	200-1-75-3-1-6-600	5.36	5.37	1.00*	99	250-2-75-3-1-6-600	20.82	21.22	0.98
28	200-1-75-5-1-6-600	5.34	5.37	0.99	100	250-2-75-5-1-6-600	20.68	21.22	0.97
29	200-1-60-3-2-6-600	5.36	5.37	1.00*	101	250-2-60-3-2-6-600	20.94	21.22	0.99
30	200-1-60-5-2-6-600	5.22	5.37	0.97	102	250-2-60-5-2-6-600	20.91	21.22	0.99
31	200-1-75-3-2-6-600	5.18	5.37	0.96	103	250-2-75-3-2-6-600	20.80	21.22	0.98
32	200-1-75-5-2-6-600	5.11	5.37	0.95	104	250-2-75-5-2-6-600	20.71	21.22	0.98
33	200-1-60-3-1-8-600	5.37	5.37	1.00*	105	250-2-60-3-1-8-600	20.97	21.22	0.99
34	200-1-60-5-1-8-600	5.33	5.37	0.99	106	250-2-60-5-1-8-600	20.93	21.22	0.99
35	200-1-75-3-1-8-600	5.36	5.37	1.00*	107	250-2-75-3-1-8-600	20.79	21.22	0.98
36	200-1-75-5-1-8-600	5.29	5.37	0.98	108	250-2-75-5-1-8-600	20.72	21.22	0.98
37	200-1-60-3-2-8-600	5.09	5.37	0.95	109	250-2-60-3-2-8-600	20.80	21.22	0.98
38	200-1-60-5-2-8-600	4.94	5.37	0.92	110	250-2-60-5-2-8-600	20.69	21.22	0.98
39	200-1-75-3-2-8-600	4.91	5.37	0.91	111	250-2-75-3-2-8-600	20.54	21.22	0.97
40	200-1-75-5-2-8-600	4.74	5.37	0.88	112	250-2-75-5-2-8-600	20.49	21.22	0.97
41	200-2-60-3-1-6-600	14.30	14.57	0.98	113	250-2-60-3-1-12-600	20.59	21.22	0.97
42	200-2-60-5-1-6-600	14.17	14.57	0.97	114	250-2-60-5-1-12-600	20.49	21.22	0.97
43	200-2-75-3-1-6-600	14.04	14.57	0.96	115	250-2-75-3-1-12-600	20.38	21.22	0.96
44	200-2-75-5-1-6-600	13.85	14.57	0.95	116	250-2-75-5-1-12-600	20.04	21.22	0.94
45	200-2-60-3-2-6-600	13.90	14.57	0.95	117	250-2-60-3-2-12-600	19.75	21.22	0.93
46	200-2-60-5-2-6-600	13.73	14.57	0.94	118	250-2-60-5-2-12-600	18.73	21.22	0.88
47	200-2-75-3-2-6-600	13.59	14.57	0.93	119	250-2-75-3-2-12-600	18.85	21.22	0.89
48	200-2-75-5-2-6-600	13.40	14.57	0.92	120	250-2-75-5-2-12-600	17.74	21.22	0.84
49	200-2-60-3-1-8-600	14.05	14.57	0.96	121	250-3-60-3-1-6-600	36.01	36.73	0.98
50	200-2-60-5-1-8-600	13.88	14.57	0.95	122	250-3-60-5-1-6-600	35.88	36.73	0.98
51	200-2-75-3-1-8-600	13.74	14.57	0.94	123	250-3-75-3-1-6-600	35.39	36.73	0.96
52	200-2-75-5-1-8-600	13.54	14.57	0.93	124	250-3-75-5-1-6-600	35.39	36.73	0.96
53	200-2-60-3-2-8-600	13.48	14.57	0.93	125	250-3-60-3-2-6-600	35.57	36.73	0.97
54	200-2-60-5-2-8-600	13.22	14.57	0.91	126	250-3-60-5-2-6-600	35.39	36.73	0.96
55	200-2-75-3-2-8-600	13.12	14.57	0.90	127	250-3-75-3-2-6-600	35.39	36.73	0.96
56	200-2-75-5-2-8-600	12.86	14.57	0.88	128	250-3-75-5-2-6-600	35.39	36.73	0.96
57	200-3-60-3-1-6-600	23.54	23.68	0.99	129	250-3-60-3-1-8-600	35.82	36.73	0.98

58	200-3-60-5-1-6-600	23.39	23.68	0.99	130	250-3-60-5-1-8-600	35.57	36.73	0.97
59	200-3-75-3-1-6-600	23.71	23.68	1.00*	131	250-3-75-3-1-8-600	35.39	36.73	0.96
60	200-3-75-5-1-6-600	23.46	23.68	0.99	132	250-3-75-5-1-8-600	35.39	36.73	0.96
61	200-3-60-3-2-6-600	22.95	23.68	0.97	133	250-3-60-3-2-8-600	35.05	36.73	0.95
62	200-3-60-5-2-6-600	22.66	23.68	0.96	134	250-3-60-5-2-8-600	35.39	36.73	0.96
63	200-3-75-3-2-6-600	23.06	23.68	0.97	135	250-3-75-3-2-8-600	35.39	36.73	0.96
64	200-3-75-5-2-6-600	22.67	23.68	0.96	136	250-3-75-5-2-8-600	35.39	36.73	0.96
65	200-3-60-3-1-8-600	23.14	23.68	0.98	137	250-3-60-3-1-12-600	34.75	36.73	0.95
66	200-3-60-5-1-8-600	22.91	23.68	0.97	138	250-3-60-5-1-12-600	35.57	36.73	0.97
67	200-3-75-3-1-8-600	23.16	23.68	0.98	139	250-3-75-3-1-12-600	35.39	36.73	0.96
68	200-3-75-5-1-8-600	22.86	23.68	0.97	140	250-3-75-5-1-12-600	35.39	36.73	0.96
69	200-3-60-3-2-8-600	22.18	23.68	0.94	141	250-3-60-3-2-12-600	33.36	36.73	0.91
70	200-3-60-5-2-8-600	21.81	23.68	0.92	142	250-3-60-5-2-12-600	35.39	36.73	0.96
71	200-3-75-3-2-8-600	22.23	23.68	0.94	143	250-3-75-3-2-12-600	35.39	36.73	0.96
72	200-3-75-5-2-8-600	21.83	23.68	0.92	144	250-3-75-5-2-12-600	35.39	36.73	0.96

305   Note: M_{slots} = bending capacity of slotted web channel, M_{solid} = bending capacity of solid web channel, * = numerical errors

306   **5   Proposed design rules for distortional buckling**

307   This section aims to improve the available Direct Strength Method (DSM) based distortional

308   buckling design equations. DSM is an alternative design method and the ultimate capacities

309   can be determined from the elastic buckling and yielding capacities. North American

310   specification for design of cold-formed structural members, AISI S100 [27], and Australian

311   and New Zealand Standard for cold-formed steel structures, AS/NZ 4600 [28] provide the

312   DSM design guidelines to predict the flexural capacity of CFS beams subject to local buckling

313   and distortional buckling. The ultimate bending capacity for distortional buckling (M_{bd}) can be

314   determined from Eqs. 1 and 2.

315   For $\lambda_d \leq 0.673$, $M_{bd} = M_y$ (1)

316   For $\lambda_d > 0.673$, $M_{bd} = \left[1 - 0.22\left(\frac{M_{od}}{M_y}\right)^{0.5}\right]\left(\frac{M_{od}}{M_y}\right)^{0.5} M_y$ (2)

317   where $\lambda_d = \sqrt{M_y/M_{od}}$, λ_d is the non-dimensional slenderness to calculate M_{bd}, M_y is the

318   yielding moment which is the product of elastic section modulus (Z) of the section and yield

319   strength and M_{od} is the elastic distortional buckling moment.

320   The latest version of both AISI S100 [27] and AS/ NZ 4600 [28] has the provision for inelastic

321   reserve capacity for distortional buckling to account higher compressive strains in symmetric

322   CFS beams. Therefore, the inelastic reserve capacity for distortional buckling can be

323   determined for the CFS sections symmetric about the axis of bending or sections with the first

324   yield in compression using Eq. 3.

325   For $\lambda_d \leq 0.673$, $M_{bd} = M_y + \left(1 - \frac{1}{C_{yd}^2}\right)\left(M_p - M_y\right)$ (3)

326 Where M_p is the plastic moment which is the product of plastic section modulus (S) and yield

327 strength (fy) and $c_{yd} = \sqrt{0.673/\lambda_d} \leq 3$.

328 The ultimate bending capacity prediction for distortional buckling using the current DSM

329 equations (Eqs. 1, 2 and 3) is plotted in Fig. 22. It is essential to calculate the plastic moment

330 (M_p) to plot the inelastic research bending capacity. Therefore, CFS solid sections were

331 analysed to determine the elastic (Z) and plastic section modulus (S) to calculate the shape

332 factor (S/Z) which is equal to the M_p/M_y. The elastic section modulus was obtained from the

333 finite strip method-based software THIN-WALL-2 [29]. Table 7 presents the shape factor

334 values for the nine CFS solid web channels. The mean shape factor value for CFS solid web

335 channels is 1.26 while the minimum value for the shape factor is 1.21. Therefore, as a

336 conservative approach, 1.21 was selected for the analysis of the results of the parametric study.

337 Fig. 22 is also plotted with the distortional buckling test results of CFS beams reported in Yu

338 and Schafer [10] and Pham and Hancock [25]. The ultimate bending capacities for distortional

339 buckling of 27 CFS solid channels obtained from the FE analyses are plotted in the DSM curve

340 (see Fig. 23). These FE results for the CFS beams with solid web are fitting well with the DSM

341 curve for distortional buckling.

342 AISI S100 [27] and AS/NZ 4600 [28] provides DSM based design guidelines to predict the

343 ultimate bending capacity of the CFS beams with rectangular web holes. These provisions

344 cannot be applicable for this staggered slotted perforated CFS beams due to the arrangement

345 and patterns of the holes. Therefore, a simple approach is chosen where a reduction factor (q_s)

346 was proposed as a function of influencing parameters considered in the parametric study. The

347 ultimate bending capacity of the staggered slotted perforated CFS beams subject to distortional

348 buckling (M_{slots}) can be calculated by applying q_s to its corresponding bending capacity of the

349 solid CFS beams (M_{solid}) as mentioned in Eq. 4.

$$M_{slots} = M_{solid} \times q_s \qquad (4)$$

351 Using the comprehensive ultimate bending capacity data obtained for the parametric study (432

352 results), an appropriate reduction factor equation was proposed considering all influencing

353 parameters. Eq. 5 gives the proposed reduction factor equation. This equation was developed

354 and optimised through a classic genetic algorithm and using the Generalised Reduced Gradient

355 (GRG) solving method. The objective function was aimed to minimise the COV of the

356 q_s(FE)/q_s(proposed) ratios of the 432 results while maintaining the mean value equal to unity.

357 The optimisation resulted in a COV of 0.04, thus defines the satisfactory accuracy of the

358 proposed reduction factor equation. Fig. 24 depicts the comparison of the reduction factor
359 obtained from FE analysis and proposed equation.

360
$$q_s = 1 - \frac{\left[\frac{B_l}{B_f}\right]^{1.077}\left[\frac{D}{t}\right]^{0.065}\left[\frac{L_{sl}}{100}\right]^{1.023}\left[\frac{W_{sl}}{9.5}\right]^{0.555}\left[\frac{N}{n}\right]^{0.502}}{\left[\frac{f_y}{250}\right]^{0.004}}$$
(5)

361 The proposed reduction factor q_s can be adopted into the DSM equations for distortional
362 buckling of CFS beams (Eq.2 and 3). The modified DSM equations with the reduction factor
363 q_s to predict the ultimate bending capacity of CFS beams with staggered slotted perforation are
364 provided in Eqs.6 and 7.

365 For $\lambda_d > 0.673$,
$$M_{bd,slots} = \left[\left[1 - 0.22\left(\frac{M_{od}}{M_y}\right)^{0.5}\right]\left(\frac{M_{od}}{M_{y,}}\right)^{0.5} M_y\right] q_s$$
(6)

366

367 For $\lambda_d \leq 0.673$,
$$M_{bd,slots} = \left[M_y + \left(1 - \frac{1}{C_{yd}^2}\right)\left(M_p - M_y\right)\right] q_s$$
(7)

368 Where q_s can be substituted from Eq. 5.
369 Fig. 25 shows bending capacity predictions of the staggered slotted perforated CFS beams
370 obtained from the modified DSM equations (Eq.6 and 7) for distortional buckling. All 432
371 points plotted in Fig. 25 reveals a satisfactory agreement with the DSM curve. Therefore, these
372 modified DSM based design equations are suitable to predict the ultimate bending capacity of
373 staggered slotted perforated CFS beams subject to distortional buckling accurately.

374 **6   Concluding remarks**

375 CFS beams with staggered slotted perforations are widely used in steel buildings to enhance
376 the thermal performance. However, the effect of incorporating staggered slotted perforations
377 on structural performance is not fully studied yet. Therefore, this paper has presented a
378 comprehensive numerical analysis on staggered slotted perforated CFS flexural members
379 subjected to distortional buckling. A detailed parametric study using 432 models was
380 conducted to generate a wide range of ultimate bending capacity data set of CFS beams with
381 staggered slotted perforations. The results showed that the slotted perforations in the web
382 reduced the ultimate bending capacity up to 23%. Then, the results were used to modify the
383 DSM based design equations to accurately predict the ultimate bending capacity of CFS beams
384 with slotted perforations in accordance with the design rules for the solid-webbed CFS beams.
385 The modified DSM based equations resulted good accuracy in predicting the bending
386 capacities of slotted perforated channels, considering all the influencing parameters. Therefore,

387 the ultimate bending capacity of staggered slotted perforated CFS beams can be reliably
388 calculated using the modified DSM based equations.

389 *Acknowledgements*

390 The authors would like to appreciate the necessary research facilities and technical assistance
391 provided by South Ural State University and Northumbria University.

392 **References**

393 [1] T. Höglund, H. Burstrand, Slotted steel studs to reduce thermal bridges in insulated
394 walls, Thin-Walled Structures. 32 (1998) 81-109. doi:10.1016/s0263-8231(98)00028-
395 7.

396 [2] R. LaBoube, Development of cost-effective, energy-efficient steel framing: Thermal
397 performance of slit-web steel wall studs, American Iron and Steel Institute, 2006.

398 [3] J. Lipták-Váradi, Equivalent thermal conductivity of steel girders with slotted web,
399 Periodica Polytechnica Civil Engineering. 54 (2010) 163. doi:10.3311/pp.ci.2010-2.12.

400 [4] F. Liu, F. Fu, Y. Wang, Q. Liu, Fire performance of non-load-bearing light-gauge
401 slotted steel stud walls, Journal of Constructional Steel Research. 137 (2017) 228-241.
402 doi:10.1016/j.jcsr.2017.06.034.

403 [5] Kesti, Local and distortional buckling of perforated steel wall studs, PhD, Helsinki
404 University of Technology, 2000.

405 [6] N. Degtyareva, V. Degtyarev, Experimental investigation of cold-formed steel channels
406 with slotted webs in shear, Thin-Walled Structures. 102 (2016) 30-42.
407 doi:10.1016/j.tws.2016.01.012.

408 [7] V. Degtyarev, N. Degtyareva, Finite element modeling of cold-formed steel channels
409 with solid and slotted webs in shear, Thin-Walled Structures. 103 (2016) 183-198.
410 doi:10.1016/j.tws.2016.02.016.

411 [8] N. Degtyareva, P. Gatheeshgar, K. Poologanathan, S. Gunalan, M. Lawson, P. Sunday,
412 Combined bending and shear behaviour of slotted perforated steel channels: Numerical
413 studies, Journal of Constructional Steel Research. 161 (2019) 369-384.
414 doi:10.1016/j.jcsr.2019.07.008.

415 [9] C. Yu, B. Schafer, Local Buckling Tests on Cold-Formed Steel Beams, Journal Of
416 Structural Engineering. 129 (2003) 1596-1606. doi:10.1061/(asce)0733-
417 9445(2003)129:12(1596).

418 [10] C. Yu, B. Schafer, Distortional Buckling Tests on Cold-Formed Steel Beams, Journal
419 Of Structural Engineering. 132 (2006) 515-528. doi:10.1061/(asce)0733-
420 9445(2006)132:4(515).

421 [11] N. Nguyen, T. Fung, B. Young, Strength and Behavior of Cold-Formed Steel Z -
422 Sections Subjected to Major Axis Bending, Journal Of Structural Engineering. 132
423 (2006) 1632-1640. doi:10.1061/(asce)0733-9445(2006)132:10(1632).

424 [12] H. Wang, Y. Zhang, Experimental and numerical investigation on cold-formed steel C-
425 section flexural members, Journal of Constructional Steel Research. 65 (2009) 1225-
426 1235. doi:10.1016/j.jcsr.2008.08.007.

427 [13] C. Yu, B. Schafer, Simulation of cold-formed steel beams in local and distortional
428 buckling with applications to the direct strength method, Journal of Constructional Steel
429 Research. 63 (2007) 581-590. doi:10.1016/j.jcsr.2006.07.008.

430 [14] R. Siahaan, P. Keerthan, M. Mahendran, Finite element modeling of rivet fastened
431 rectangular hollow flange channel beams subject to local buckling, Engineering
432 Structures. 126 (2016) 311-327. doi:10.1016/j.engstruct.2016.07.004.

433 [15] R. Siahaan, M. Mahendran, P. Keerthan, Section moment capacity tests of rivet
434 fastened rectangular hollow flange channel beams, Journal Of Constructional Steel
435 Research. 125 (2016) 252-262. doi:10.1016/j.jcsr.2016.06.021.

436 [16] R. Siahaan, M. Mahendran, P. Keerthan, Section moment capacity tests of rivet
437 fastened rectangular hollow flange channel beams, Journal Of Constructional Steel
438 Research. 125 (2016) 252-262. doi:10.1016/j.jcsr.2016.06.021.

439 [17] C. Moen, A. Schudlich, A. von der Heyden, Experiments on Cold-Formed Steel C-
440 Section Joists with Unstiffened Web Holes, Journal Of Structural Engineering. 139
441 (2013) 695-704. doi:10.1061/(asce)st.1943-541x.0000652.

442 [18] J. Zhao, K. Sun, C. Yu, J. Wang, Tests and direct strength design on cold-formed steel
443 channel beams with web holes, Engineering Structures. 184 (2019) 434-446.
444 doi:10.1016/j.engstruct.2019.01.062.

445 [19] J. Kesti, Uumasta rei'itetyn seinärangan mitoitustutkimus. Lisensiaatintyö, joka on
446 jätetty opinnäytteenä tarkastettavaksi tekniikan lisensiaatin tutkintoa, Teknillinen
447 Korkeakoulu, 1997. (in Finnish).

448 [20] N. Degtyareva, Review of Experimental Studies of Cold-Formed Steel Channels with
449 Slotted Webs under Bending, Procedia Engineering. 206 (2017) 875-880.
450 doi:10.1016/j.proeng.2017.10.566.

451 [21] ANSYS, Commands reference, elements reference, operations guide, Basic Analysis
452   Guide, Theory Reference for ANSYS (2019)

453 [22] B. Schafer, Z. Li, C. Moen, Computational modelling of cold-formed steel, Thin-
454   Walled Structures. 48 (2010) 752-762. doi:10.1016/j.tws.2010.04.008.

455 [23] B. Schafer, T. Peköz, Computational modeling of cold-formed steel: characterizing
456   geometric imperfections and residual stresses, Journal of Constructional Steel
457   Research. 47 (1998) 193-210. doi:10.1016/s0143-974x(98)00007-8.

458 [24] D. Camotim, N. Silvestre, GBT based analysis of the distortional postbuckling
459   behaviour of cold-formed steel Z-section columns and beams, in: Fourth International
460   Conference On Thin-Walled Structures, Loughborough, 2004: pp. 243-250.

461 [25] C. Pham, G. Hancock, Experimental Investigation and Direct Strength Design of High-
462   Strength, Complex C-Sections in Pure Bending, Journal of Structural Engineering. 139
463   (2013) 1842-1852. doi:10.1061/(asce)st.1943-541x.0000736.

464 [26] C. Pham, Direct Strength Method of Design of Cold-Formed Sections in shear, and
465   Combined bending and shear, Ph.D, The University of Sydney, 2010.

466 [27] American Iron and Steel Institute (AISI), Specifications for the cold-formed steel
467   structural members, cold-formed steel design manual, AISI S100, Washington DC,
468   USA, 2016.

469 [28] Standards Australia, AS/NZS 4600:2018: Cold-formed steel structures. Sydney,
470   Australia, 2018.

471 [29] V. V. Nguyen, G. J. Hancock, C. H. Pham, Development of the Thin-Wall-2 program
472   for buckling analysis of thin-walled sections under generalised loading, Proceedings of
473   the eighth international conference on advances in steel structures, Lisbon, Portugal,
474   2015.

475

476

477

478

479

480
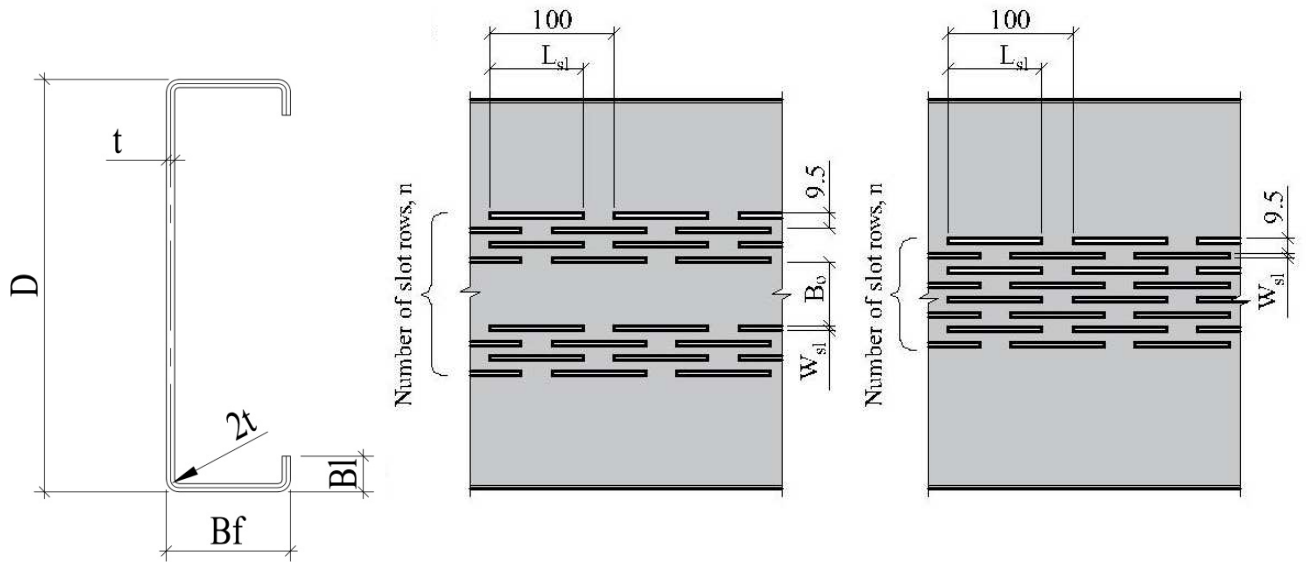
Fig. 1. CFS beams with slotted perforations
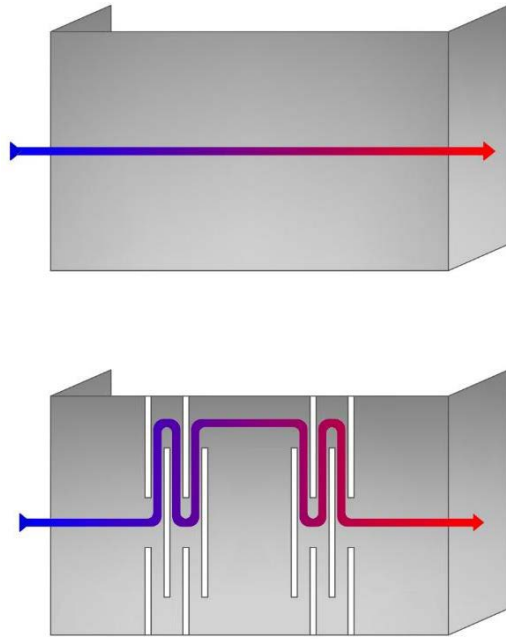
Fig. 2. Heat flow path in solid and slotted web CFS beams
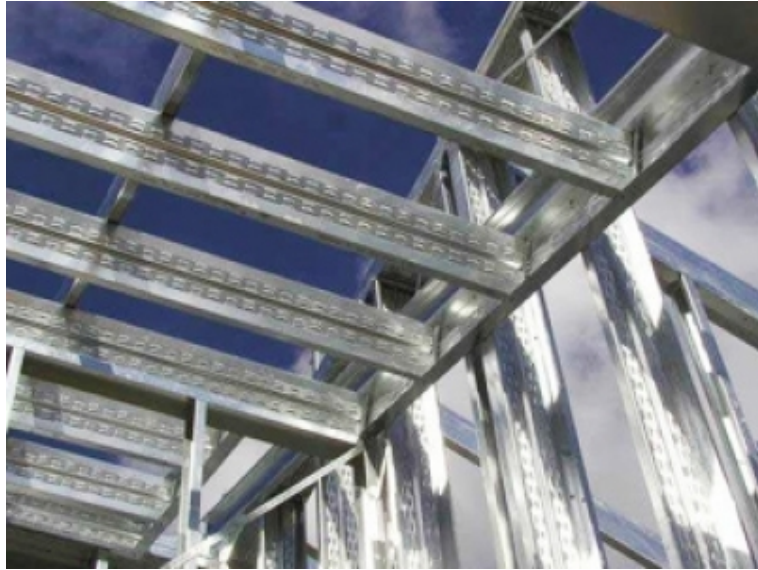
Fig. 3. Application of slotted perforated CFS beams
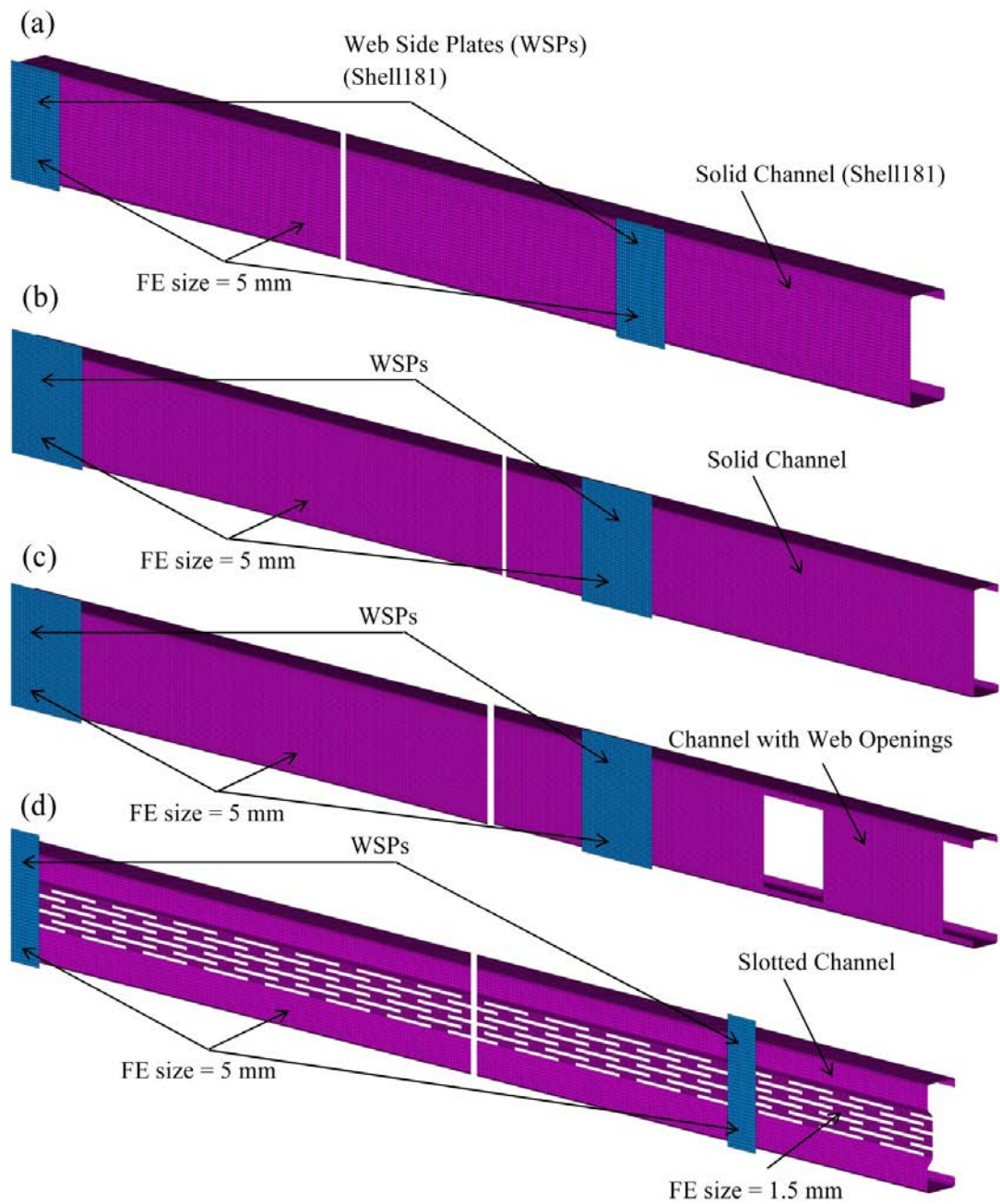
Fig. 4. Developed FE models to validate the test results of: (a) Pham [25]; (b, c) Moen [17]; (d) Kesti [19]

Translations of marked
WSP and web nodes
coupled in x, y and z

Translations and rotations of marked top and bottom
flanges nodes restrained in x and z, respectively

Force

Rotations of WSP end
nodes coupled in y

Symmetry

WSP node
restrained in y

Contact between WSP and
channel web. All WSP
nodes restrained in x

Translations of marked
WSP and web nodes
coupled in x, y and z

Fig. 5. Simulated boundary conditions in FE model to validate Pham's [25] tests
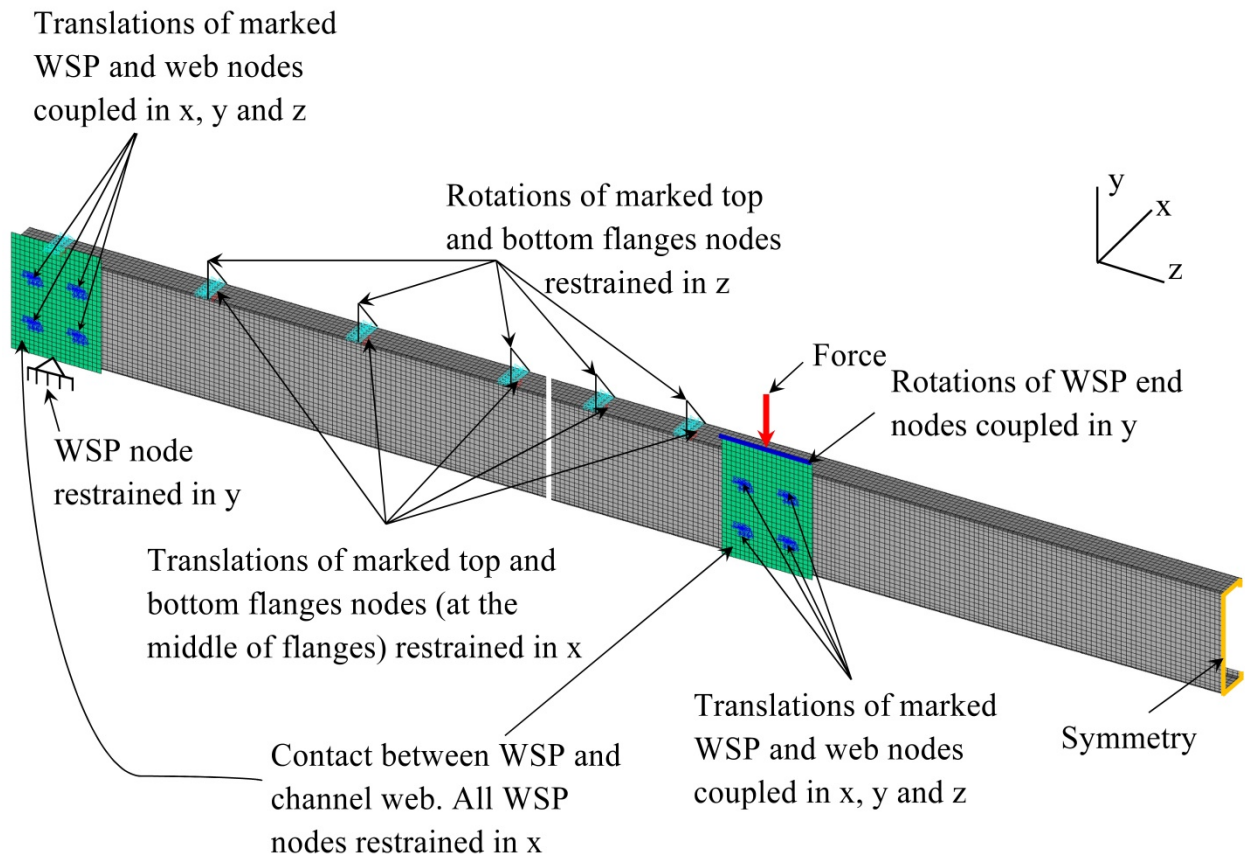
Fig. 6. Simulated boundary conditions in FE model to validate Moen's [17] tests
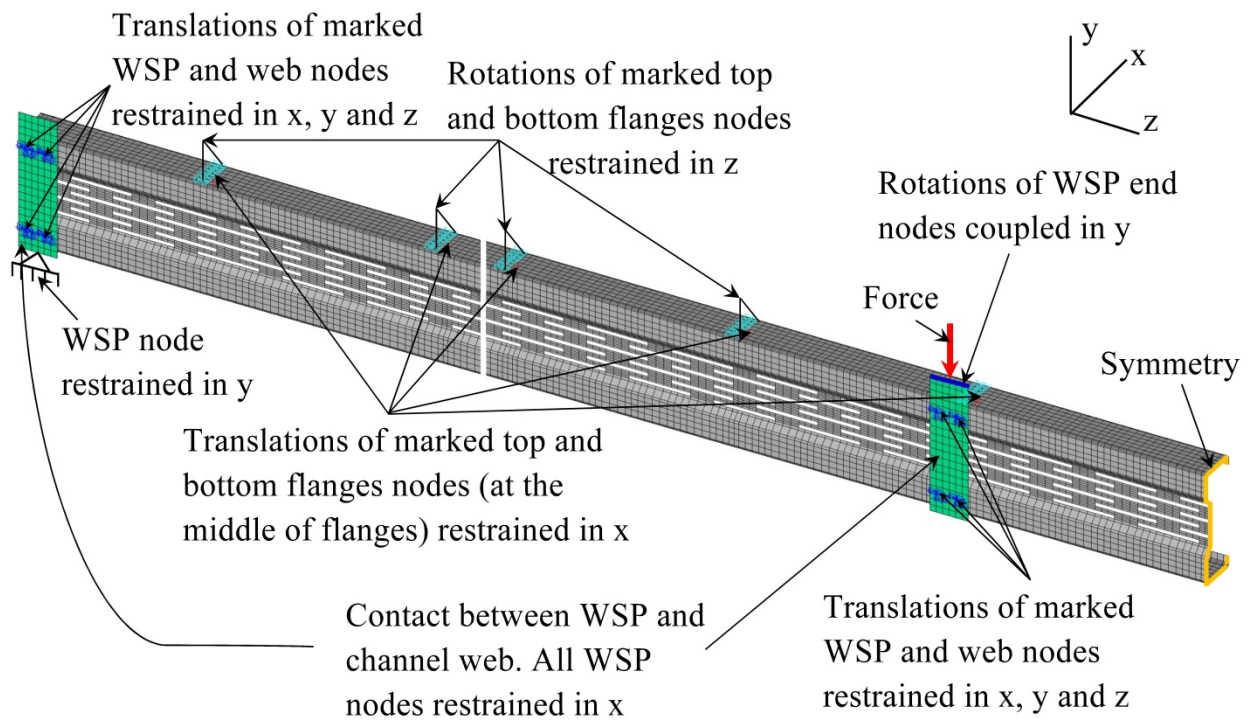
Fig. 7. Simulated boundary conditions in FE model to validate Kesti's [19] tests
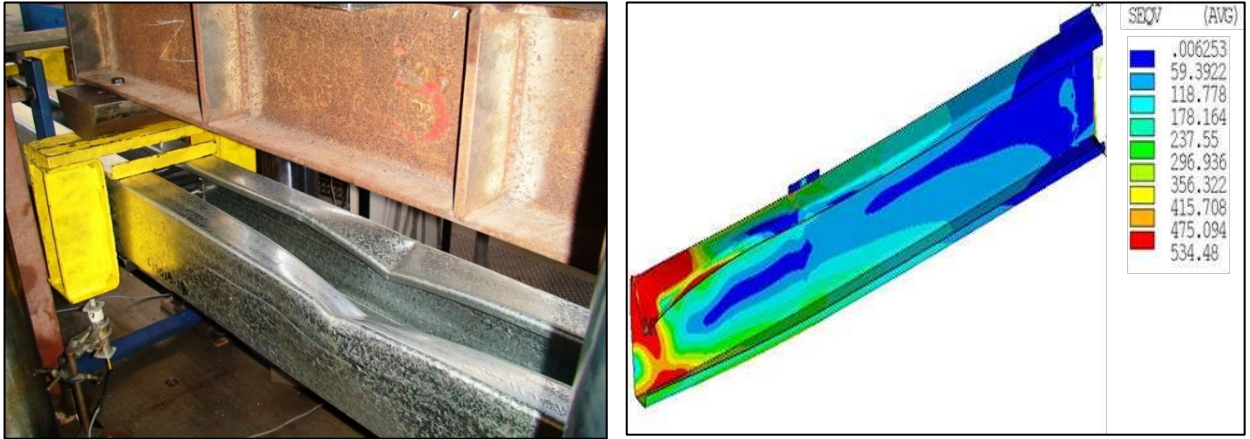
Fig. 8. Failure mode comparison between test [26] and FE models of the tested specimen C15019-Mw and FE model
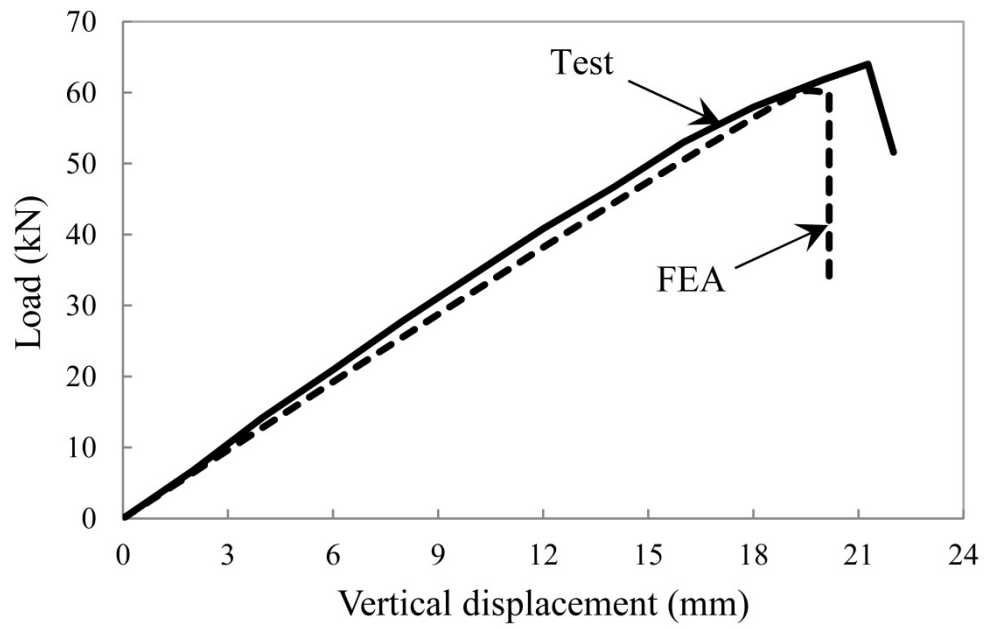
Fig. 9. Load-vertical displacement behaviour obtained for the specimen C15019-Mw from test [25] and FE analysis.
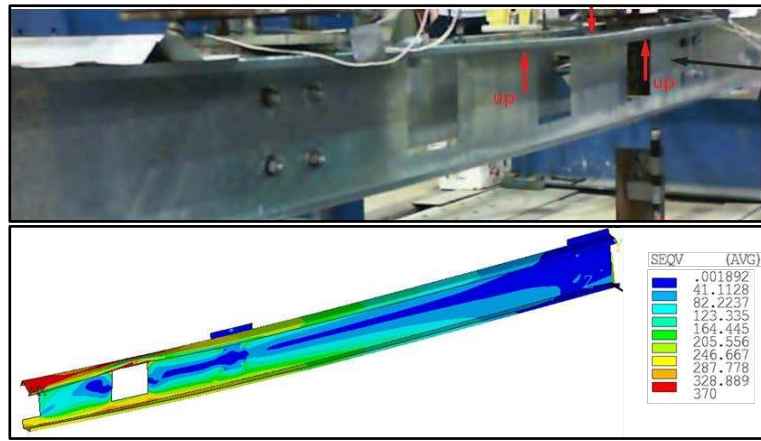
(a) H0.9-3.1
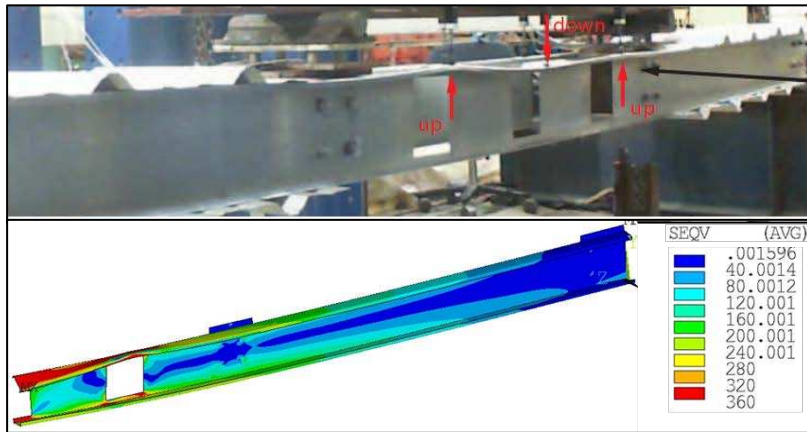
(b) H0.8-1.2
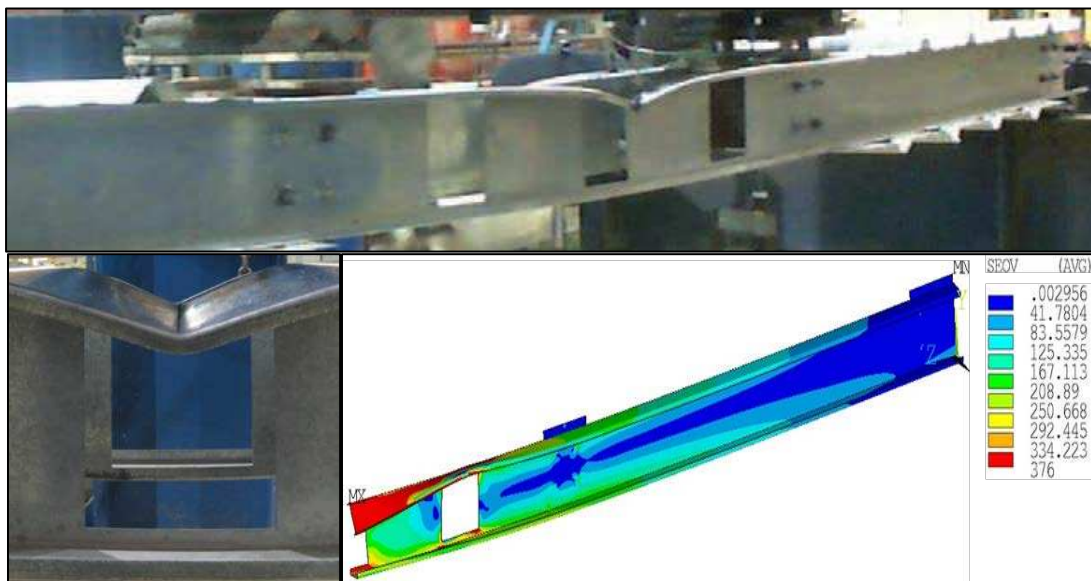
(b) H0.8-3.2

Fig.10. Failure modes comparison between test [17] and FE models

Slot width (W_{sl}), mm
(3, 5)

Thickness (t), mm
(1, 2, 3)

Number of slot rows (W_{sl}), mm
(6, 8, 12)

$\square$ – $\square$ – $\square$ – $\square$ – $\square$ – $\square$ – $\square$

Slot length (L_{sl}), mm
(60, 75)

Yield strength (f_y), MPa
(300, 500, 600)

Section depth (D), mm
(150, 200, 250)

Number of slot row groups (N)
(1, 2)
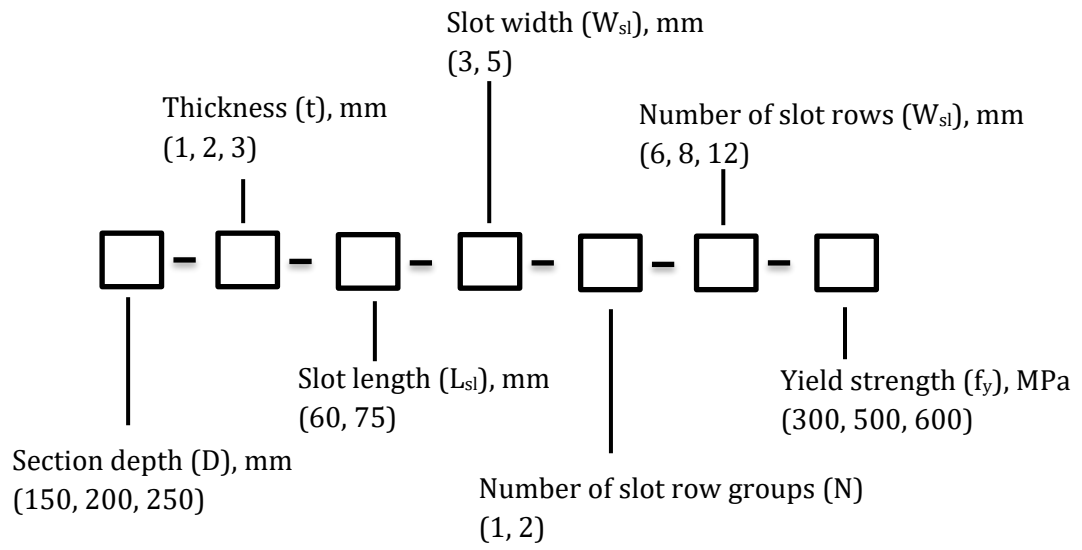
Fig. 11. FE model nomenclature for parametric study

(a) Solid Channel

Shell181

FE size = 5 mm

(b) Slotted Channel with One Perforated Region

Shell181

FE size = 5 mm

FE size = 1.5 mm

(c) Slotted Channel with Two Perforated Regions

Shell181

FE size = 5 mm

FE size = 1.5 mm
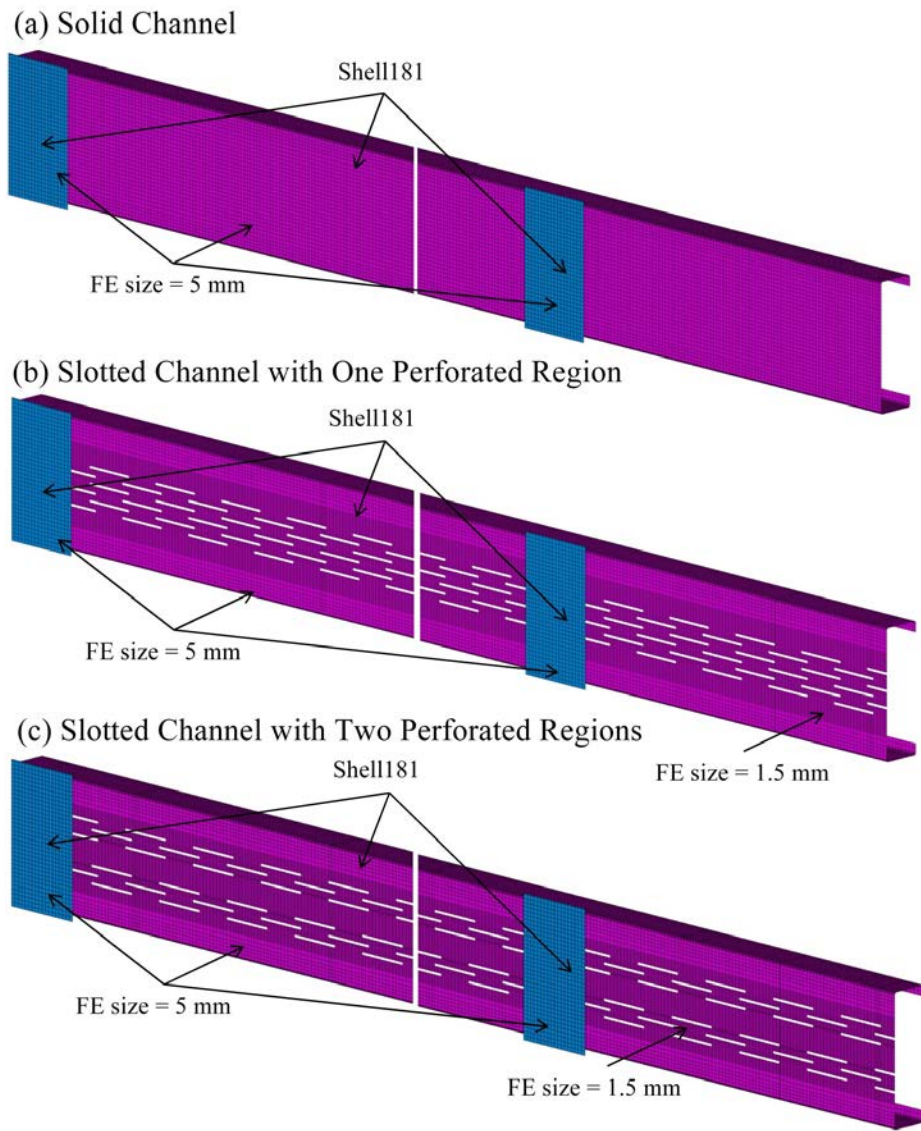
Fig. 12. FE models of 4800 mm long beam with staggered slotted perforations are provided in entire span (for parametric study)

(a) Solid Channel

Shell181

FE size = 5 mm

(b) Slotted Channel with One Perforated Region

Shell181

FE size = 5 mm

FE size = 1.5 mm

(c) Slotted Channel with Two Perforated Regions

Shell181

FE size = 5 mm

FE size = 1.5 mm
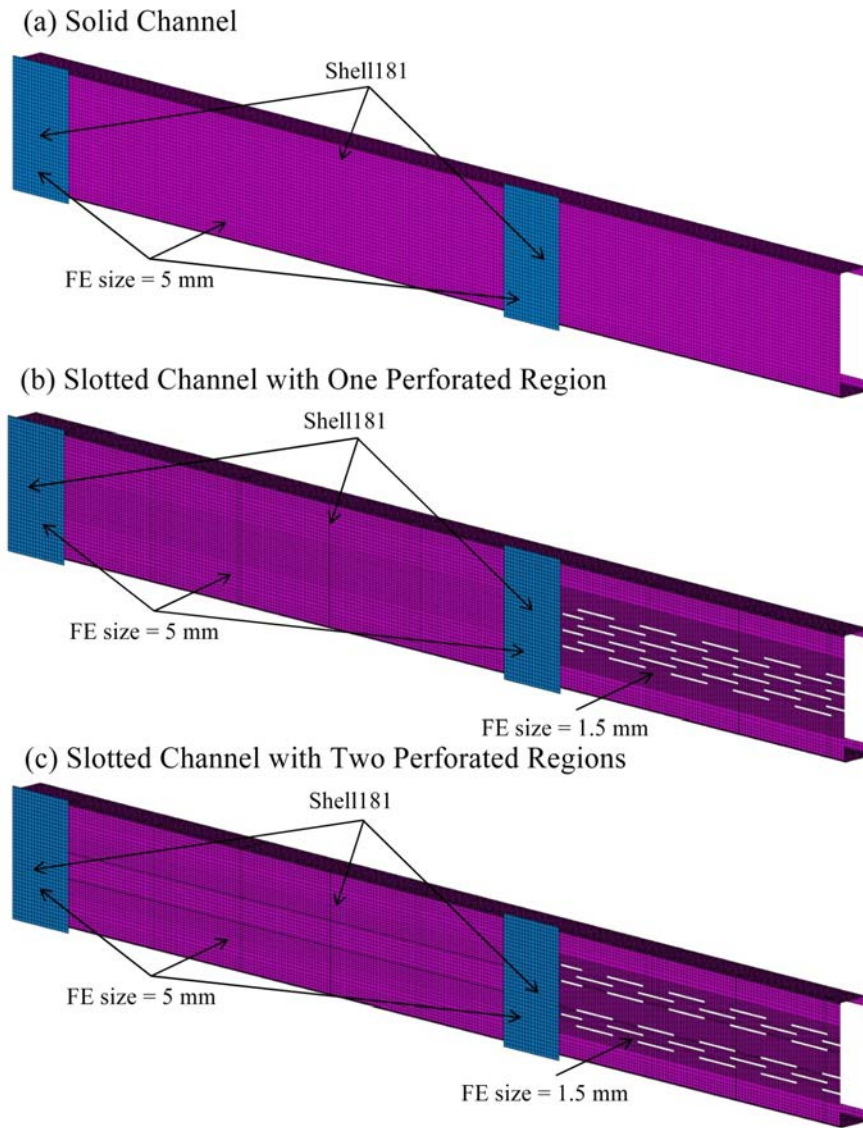
Fig. 13. FE models of 2600 mm long beam with staggered slotted perforations are only provided in the mid-span (for parametric study)
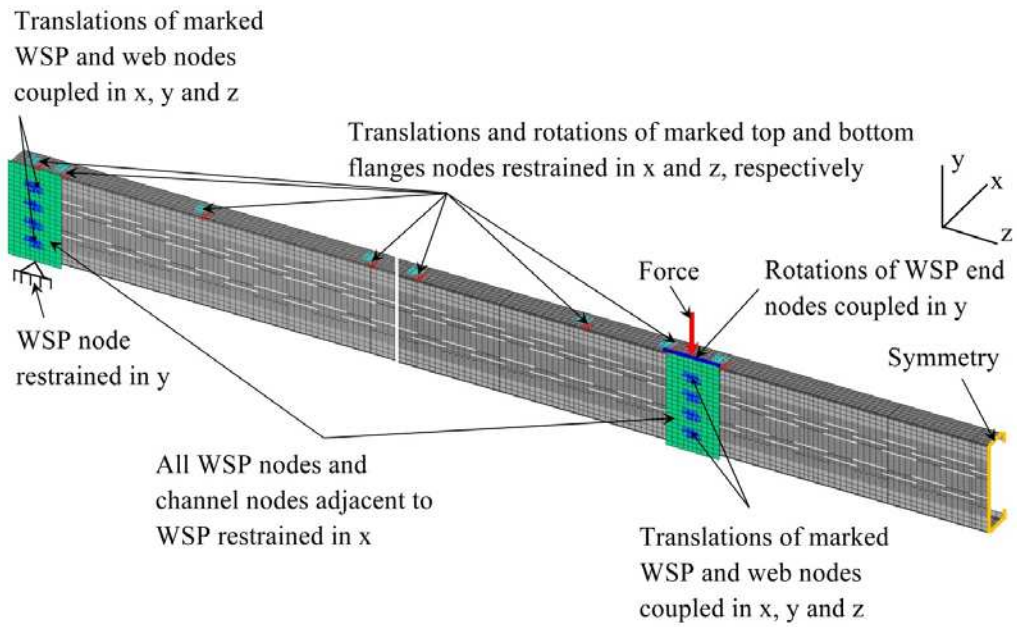
Fig. 14. Boundary conditions for FE models of 4800 mm long beams
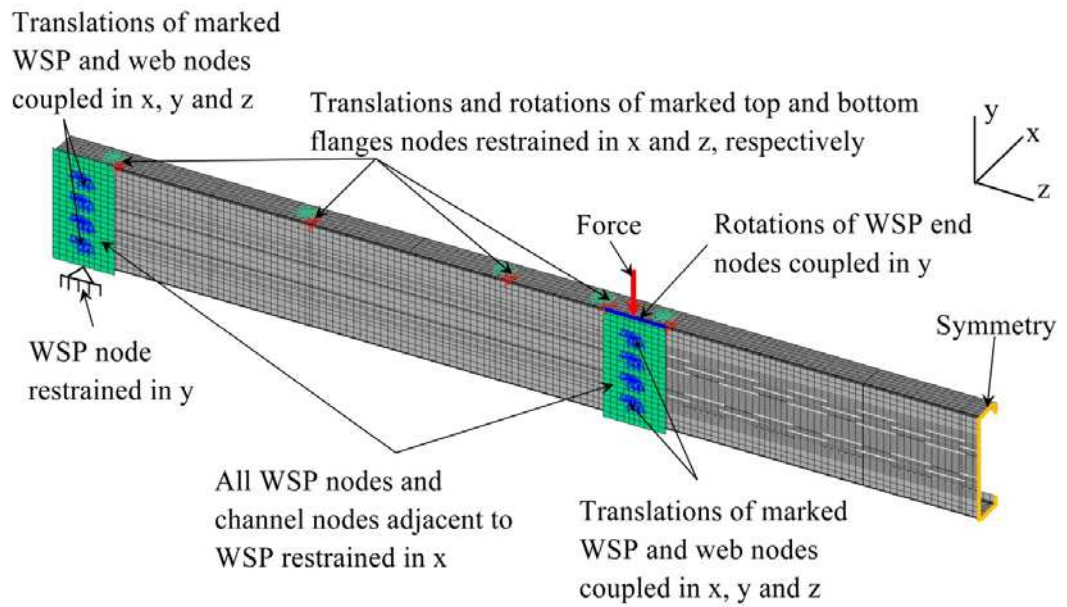
Fig. 15. Boundary conditions for FE models of 2600 mm long beams (for parametric study)
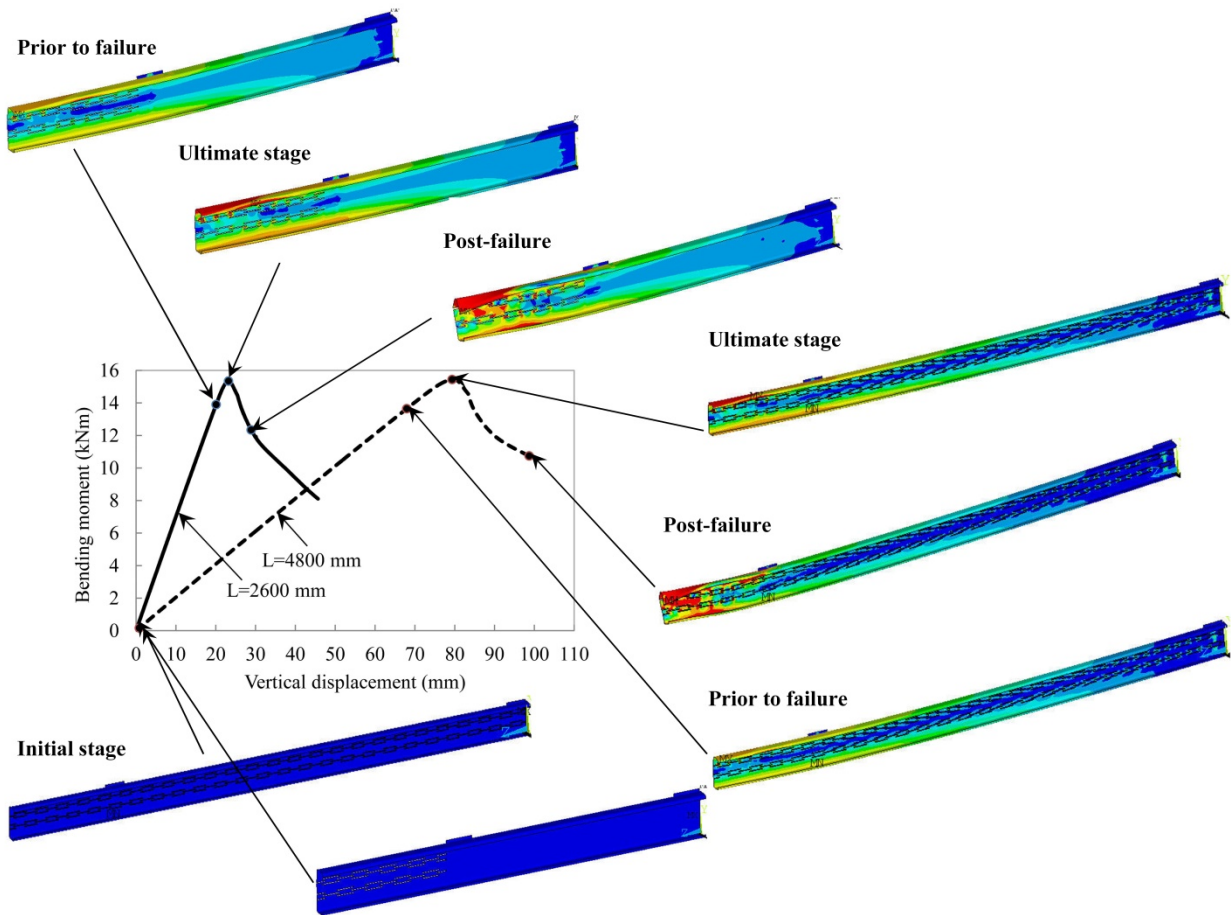
Fig. 16. Load-deflection plot of slotted channel 150-3-60-3-2-6-600 and its behavior at different stages.
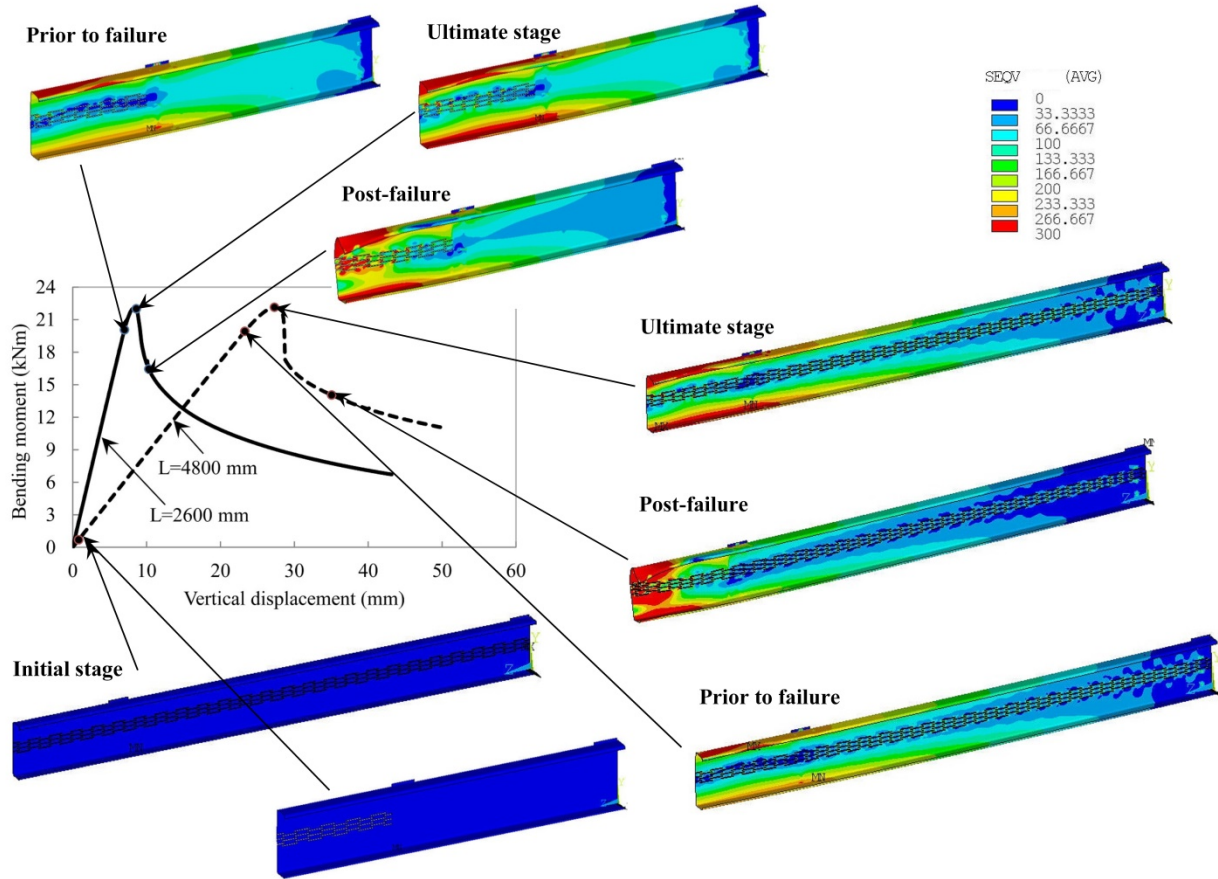
Fig. 17. Load-deflection plot of slotted channel 250-3-60-3-1-6-300 and its behavior at different stages.
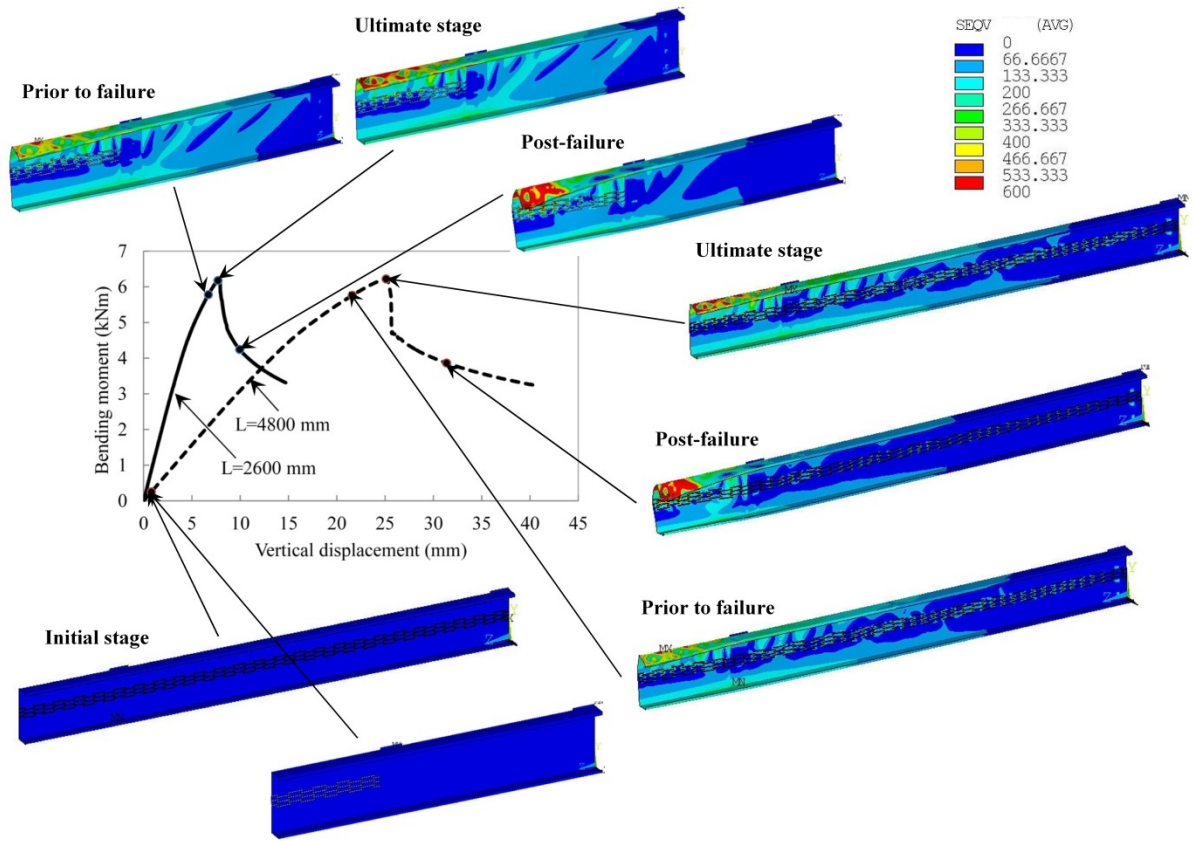
Fig. 18. Load-deflection plot of slotted channel 250-1-60-3-1-6-600 and its behavior at different stages.
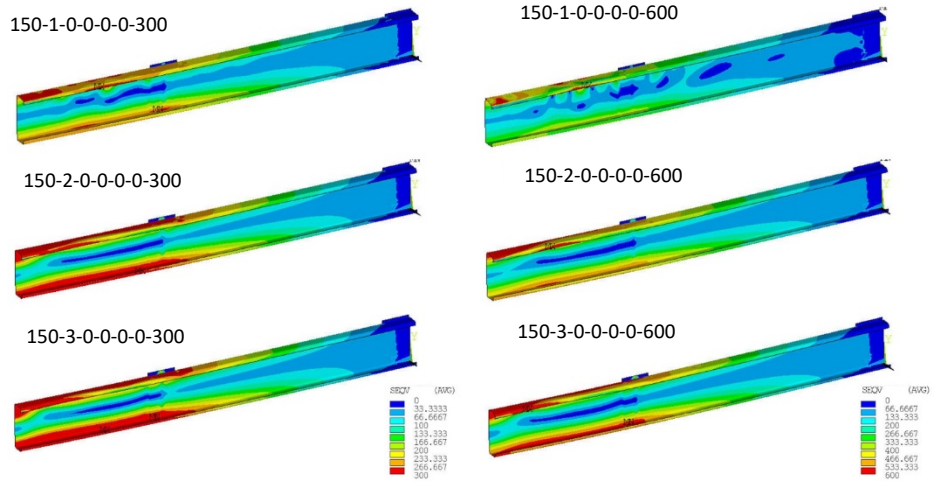
(a) Solid web CFS channels
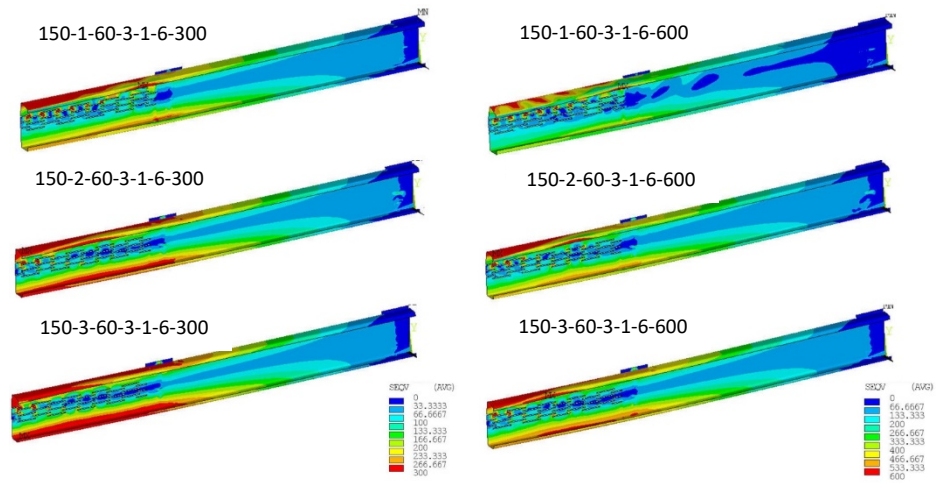
(b) Staggered slotted perforated channels

Fig. 19. Von misses stress failure pattern for 150 mm section depth solid and slotted perforated channels.
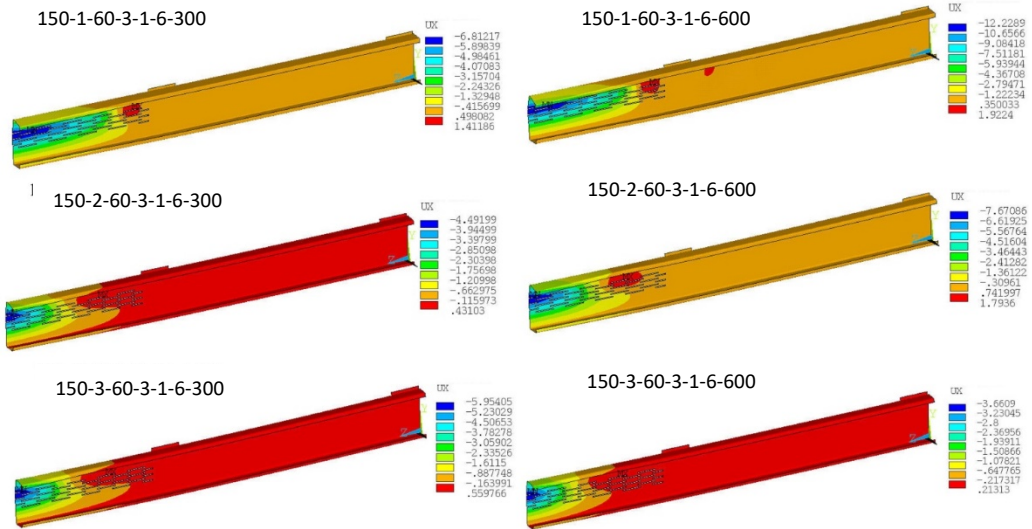
(a) 150 mm section depth CFS channels
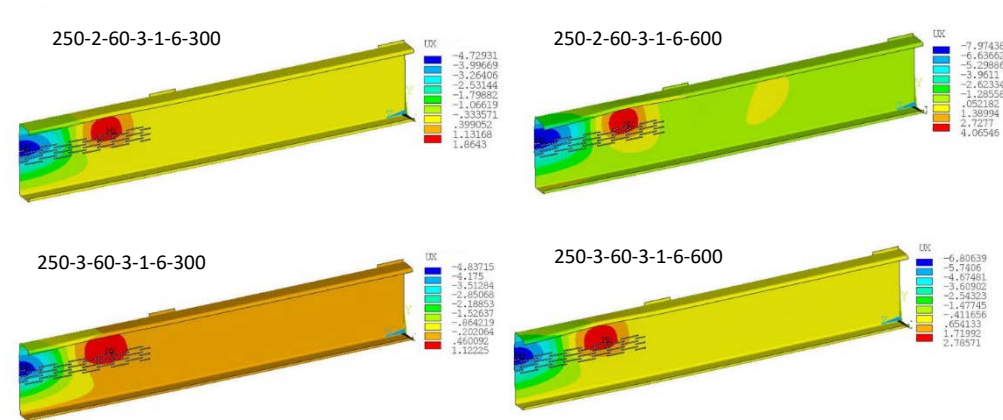
(b) 250 mm section depth CFS channels

Fig. 20. Deformation failure pattern of 150 and 250 mm section depth CFS channels with staggered slotted perforations

(a) Section depth

(b) Thickness

(c) Yield strength

(d) Slot length

(e) Slot rows and slot row groups

(f) Slot width
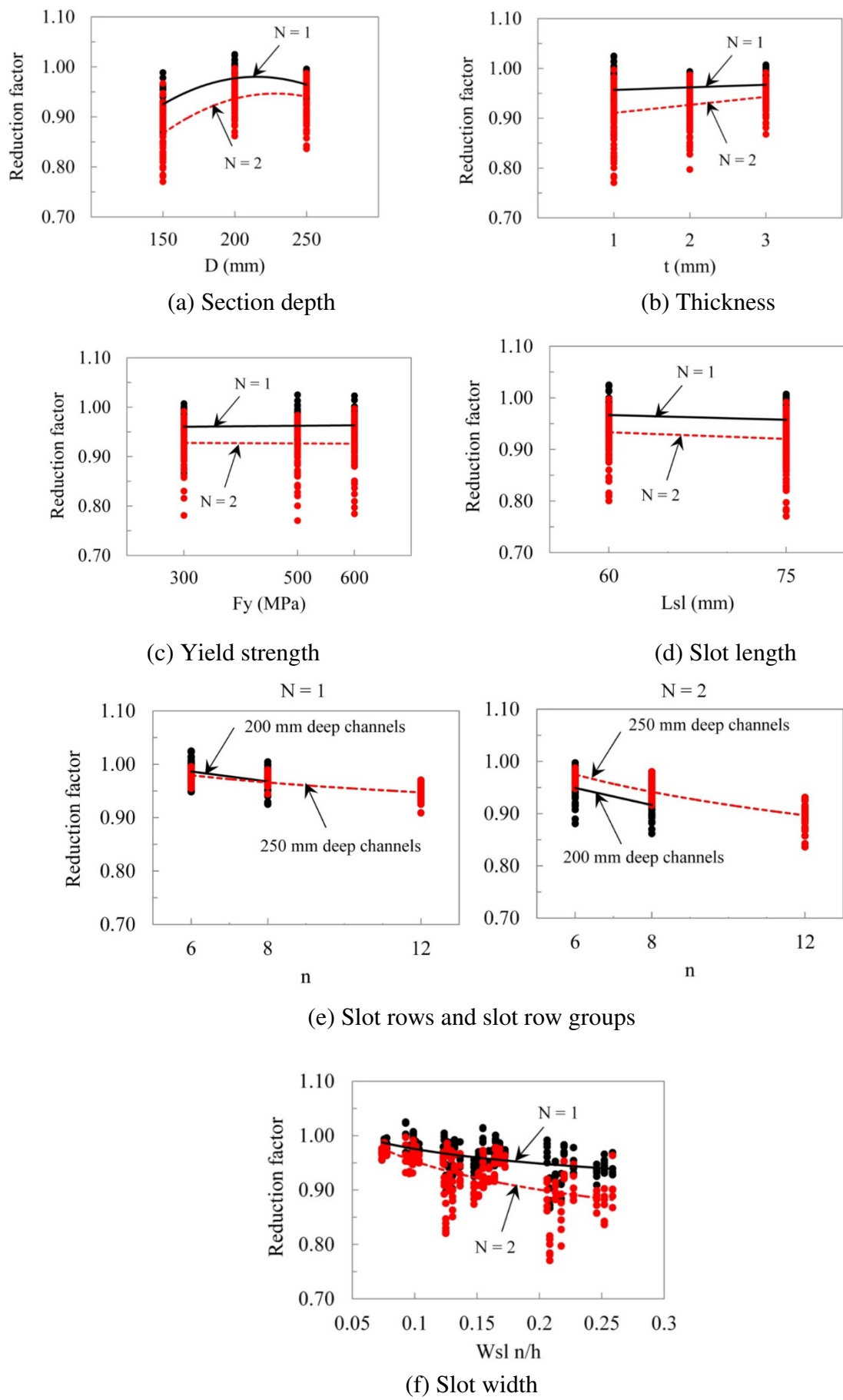
Fig. 21. Variation of reduction factor with influencing parameters.
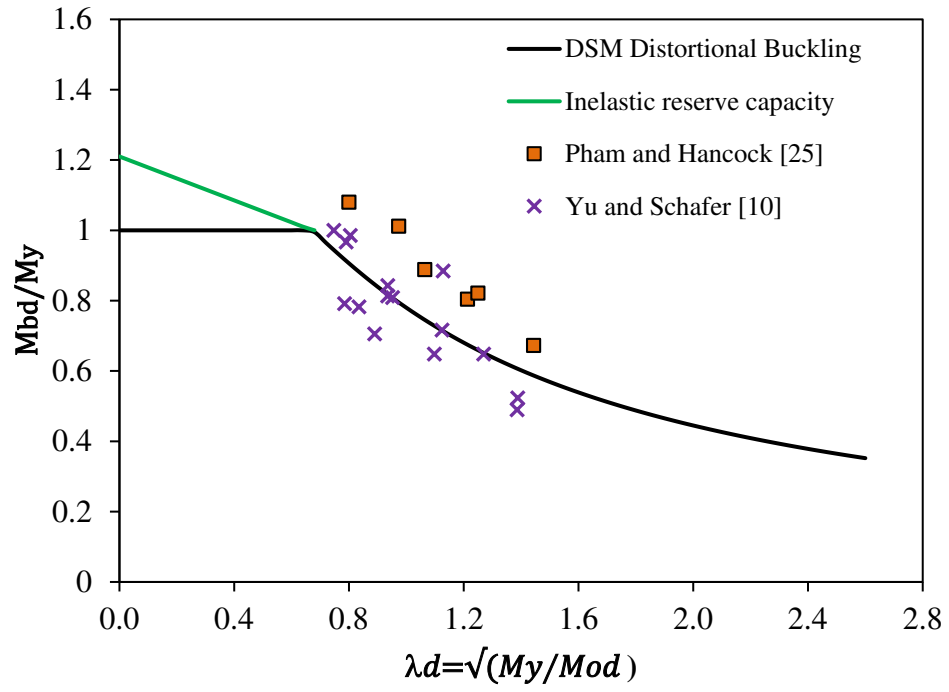
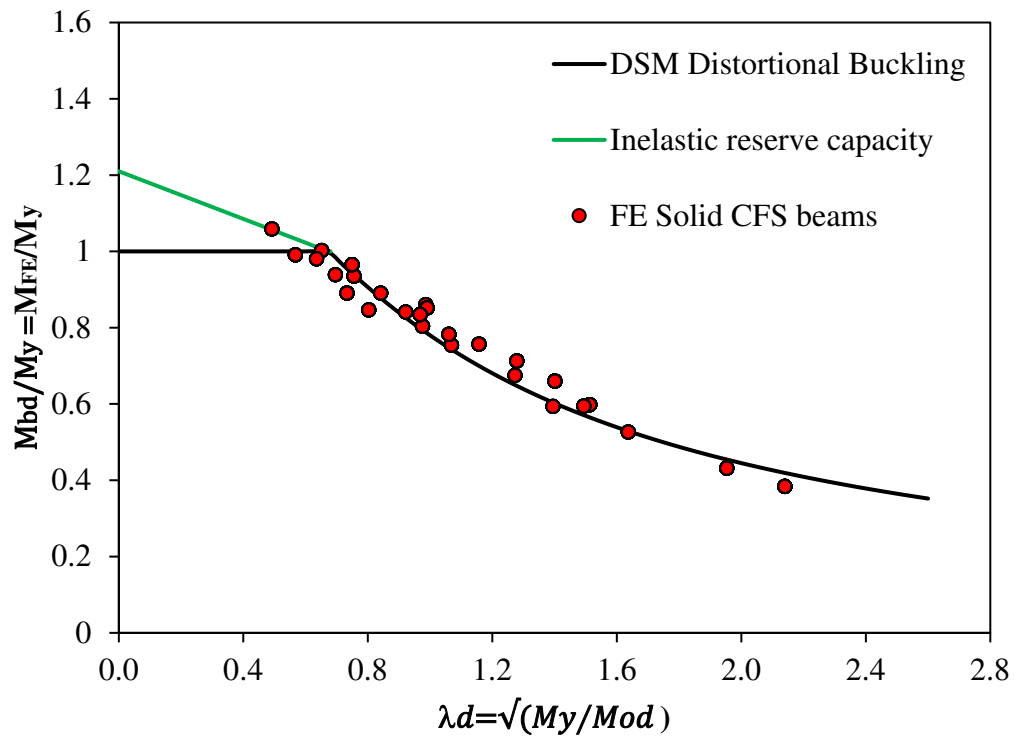Fig. 22. DSM for distortional buckling and test results [10, 25]

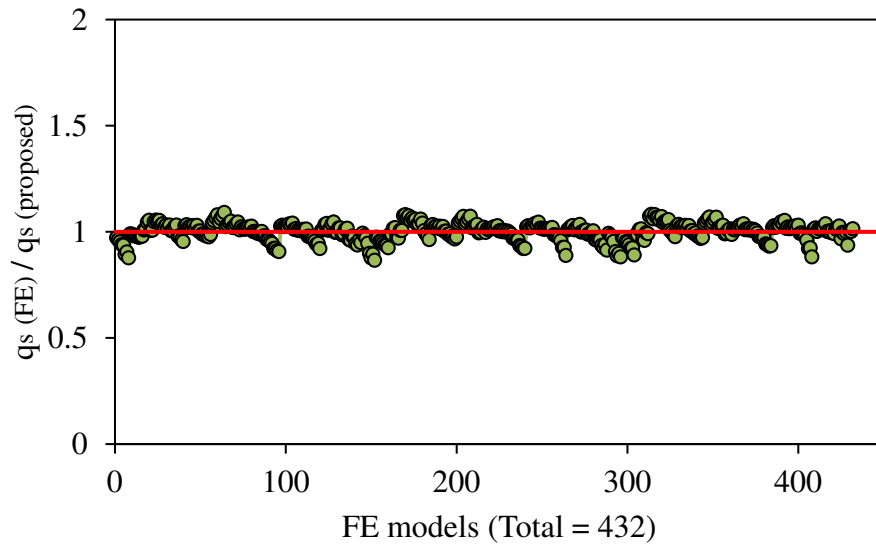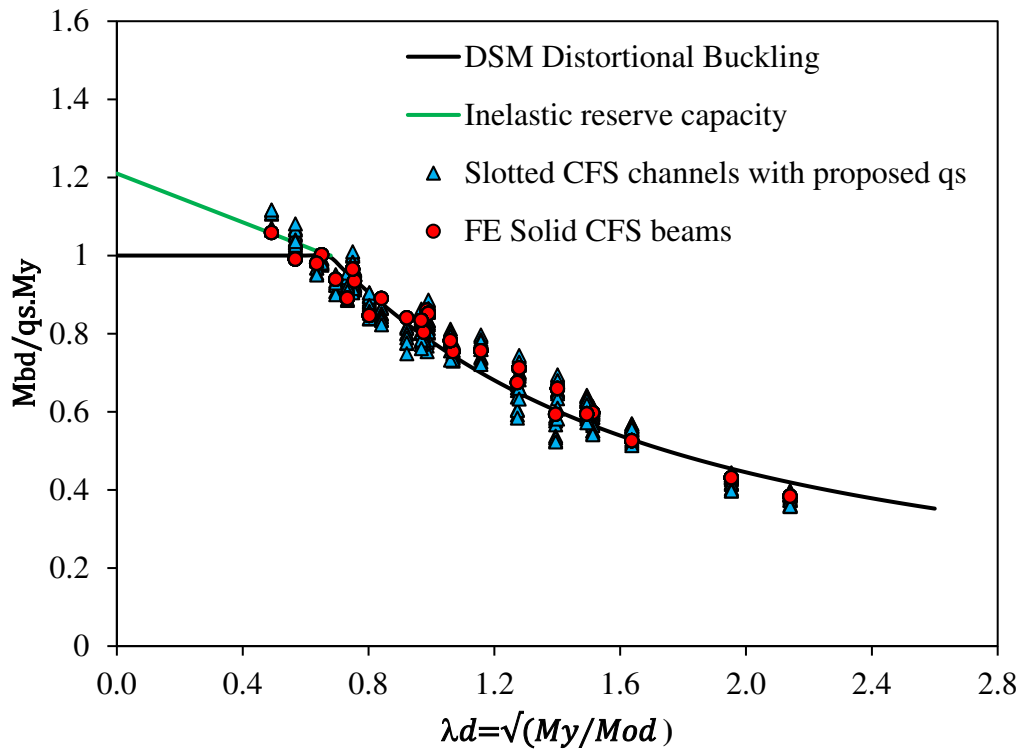Fig. 23. FE capacity predictions for CFS solid web beams

Fig. 24. Comparison of the reduction factor obtained from FE and proposed equation

For solid CFS channels, $q_s = 1$　　　　For slotted perforated CFS channels, q_s is from Eq. 5

Fig. 25. Bending capacity predictions for slotted perforated beams with proposed q_s along with corresponding solid web beams